Science Arts & Métiers (SAM)
is an open access repository that collects the work of Arts et Métiers Institute of Technology researchers and makes it freely available over the web where possible.

This is an author-deposited version published in: https://sam.ensam.eu
Handle ID: .http://hdl.handle.net/10985/19135

To cite this version :

C. CRUZ, Gilles REGNIER, Francisco CHINESTA SORIA - Review on the Brownian Dynamics Simulation of Bead-Rod-Spring Models Encountered in Computational Rheology - Archives of Computational Methods in Engineering - Vol. 19, n°2, p.227-259 - 2012

Any correspondence concerning this service should be sent to the repository Administrator : scienceouverte@ensam.eu

Review on the Brownian Dynamics Simulation of Bead-Rod-Spring Models Encountered in Computational Rheology

C. Cruz · F. Chinesta · G. Régnier

Abstract Kinetic theory is a mathematical framework intended to relate directly the most relevant characteristics of the molecular structure to the rheological behavior of the bulk system. In other words, kinetic theory is a micro-to-macro approach for solving the flow of complex fluids that circumvents the use of closure relations and offers a better physical description of the phenomena involved in the flow processes. Cornerstone models in kinetic theory employ beads, rods and springs for mimicking the molecular structure of the complex fluid. The generalized bead-rod-spring chain includes the most basic models in kinetic theory: the freely jointed bead-spring chain and the freely-jointed bead-rod chain. Configuration of simple coarse-grained models can be represented by an equivalent Fokker-Planck (FP) diffusion equation, which describes the evolution of the configuration distribution function in the physical and configurational spaces. FP equation can be a complex mathematical object, given its multidimensionality, and solving it explicitly can become a difficult task. Even more, in some cases, obtaining an equivalent FP equation is not possible given the complexity of the coarse-grained molecular model. Brownian dynamics can be employed as an alternative extensive numerical method for approaching the configuration distribution function of a given kinetic-theory model that avoid obtaining and/or resolving explicitly an equivalent FP equation. The validity of this discrete approach is based on the mathematical equivalence between a continuous diffusion equation and a stochastic differential equation as demonstrated by Itô in the 1940s. This paper presents a review of the fundamental issues in the BD simulation of the linear viscoelastic behavior of bead-rod-spring coarse grained models in dilute solution. In the first part of this work, the BD numerical technique is introduced. An overview of the mathematical framework of the BD and a review of the scope of applications are presented. Subsequently, the links between the rheology of complex fluids, the kinetic theory and the BD technique are established at the light of the stochastic nature of the bead-rod-spring models. Finally, the pertinence of the present state-of-the-art review is explained in terms of the increasing interest for the stochastic micro-to-macro approaches for solving complex fluids problems. In the second part of this paper, a detailed description of the BD algorithm used for simulating a small-amplitude oscillatory deformation test is given. Dynamic properties are employed throughout this work to characterise the linear viscoelastic behavior of bead-rod-spring models in dilute solution. In the third and fourth part of this article, an extensive discussion about the main issues of a BD simulation in linear viscoelasticity of diluted suspensions is tackled at the light of the classical multi-bead-spring chain model and the multi-bead-rod chain model, respectively. Kinematic formulations, integration schemes and expressions to calculate the stress tensor are revised for several classical models: Rouse and Zimm theories in the case of multi-bead-spring chains, and Kramers chain and semi-flexible filaments in the case of multi-bead-rod chains. The implemented BD technique is, on the one hand, validated in front of the analytical or exact numerical solutions known of the equivalent FP equations for those classic kinetic theory models; and, on the other hand, is control-set thanks to the analysis of the main numer-

---

C. Cruz · G. Régnier (✉)
Laboratoire des Procédés et Ingénierie en Mécanique et Matériaux (PIMM, UMR CNRS 8006), Arts et Métiers ParisTech, 151 bd de l'Hôpital, 75013 Paris, France
e-mail: gilles.regnier@ensam.eu

F. Chinesta
Corporate Foundation International Chair, Ecole Centrale de Nantes, 1 rue de la Noë, BP 92101, 44321 Nantes Cédex 3, Nantes, France

ical issues involved in a BD simulation. Finally, the review paper is closed by some concluding remarks.

Notes on Notation

Scalars	Lightface
Vectors and Tensors	Boldface
$(\mathbf{A})^{ij}$	Component ij of tensor $\mathbf{A}$
$(\mathbf{A})_t$	Tensor or vector $\mathbf{A}$ at instant t

1 Introduction

This paper presents a state-of-the-art review of the numerical methods in Brownian dynamics used to model the rheological behavior of bead-rod-spring models. Generalized bead-rod-spring models are coarse-grained representations of the molecular structure of complex fluids. In addition, bead-rod-spring models are the cornerstone of the kinetic theory, a formal framework that try to explain the flow dynamics of non-Newtonian fluids by relating the molecular structure with the bulk flow behavior. In order to reveal the intrinsic dynamic response of those coarse-grained models this article focuses on the linear viscoelastic behavior of their dilute solutions, where inter-molecular interactions are neglected.

This introductory section is decomposed in three parts. In the first one, a general view of the Brownian dynamics framework and its scope of applications are presented. In the second section, a brief outline about the rheology of complex fluids followed by its relation with the kinetic theory is presented. The inherent stochastic nature of the coarse-grained models is revealed establishing a connection with the Brownian dynamics technique. Finally, in the third section a line of argument is developed to show the interest of using the stochastic approach when solving kinetic theory problems.

1.1 Brownian Dynamics Modelling

A mathematical representation of all physical phenomena occurring in the physical world cannot be treated efficiently using only one kind of model. In general, the choice of a given modelling approach depends on the time and length scales involved in the phenomenon. For example, quantum physics is a suitable model for representing the phenomena occurring at the level of quantum particles, but probably the quantum physics framework is not the more convenient choice to model a tensile relaxation test in a polyethylene film. Today, quantum physics is the finest description of the matter (or energy). Going up in length and time scales of modelling requires different mathematical formulations with the aim of encapsulate the phenomena occurring at finer scales. For example, between the molecular and macroscopic scales, models must contain a mathematical architecture taking into account the rapid oscillations occurring at lower scales (i.e. atoms, smaller molecules or smaller particles). Brownian dynamics (BD) is precisely one of the mathematical frameworks employed for representing the physics at the micro-meso scale (1 nm–10 μm). In BD the rapid thermal oscillations at lower scales are tackled as a stochastic variable [1].

The historical motivation that inspired the development the Brownian dynamics framework was the publication of the Robert Brown's observations about the random motion of pollen particles in water. The irregular path described by those pollen particles was explained afterwards as the result of random thermal collisions between pollen particles and water molecules. By the way, a mathematic formalism describing the motion of a particle submitted to stochastic forces was introduced by the French physicist Paul Langevin [2]. In fact, a general differential stochastic equation is also known as a *Langevin equation*. Considering a Brownian particle (in the large sense, i.e. a discrete portion of matter submitted to stochastic forces coming from the surrounding homogeneous media) of mass M, the instantaneous *general Langevin equation* of motion writes:

$$M\ddot{\mathbf{r}} = -\nabla U(\mathbf{r}) - \varsigma M\dot{\mathbf{r}} + \varsigma M\boldsymbol{\kappa}(\mathbf{r}) + \mathbf{F}^{(b)} \tag{1}$$

where $\mathbf{r}$ is the particle position, ς is the specific friction coefficient, $\boldsymbol{\kappa}$ is the homogenous velocity gradient coming from the suspension at the position of the particle, U is the sum of all the particle interaction potentials (e.g. mechanical, electrostatic, magnetic) and $\mathbf{F}^{(b)}$ is the Brownian force acting on the particle. This last variable confers to the differential equation its stochastic nature. Keeping in mind that $\mathbf{F}^{(b)}$ is originated from independent thermal collisions with the surrounding particles; the central limit theorem conduct intuitively to think that $\mathbf{F}^{(b)}$ behaves following a Gaussian process. A formal definition of $\mathbf{F}^{(b)}$ in coherence with the stochastic calculus framework writes as follows:

$$\mathbf{F}^{(b)}_t = \sqrt{2k_B T \varsigma M}\,\frac{d(\mathbf{W})_t}{dt} \tag{2}$$

where k_B is the Boltzmann's constant, T is the absolute temperature and $(\mathbf{W})_t$ is a Wiener process at instant t. $(\mathbf{W})_t$ is a well-defined Gaussian process itself, hence can be defined by the first and second moments of its distribution:

$$\big\langle (\mathbf{W})_t \big\rangle = \mathbf{0} \tag{3}$$

$$\big\langle (\mathbf{W})_{t_1} \otimes (\mathbf{W})_{t_2} \big\rangle = \min(t_1, t_2)\boldsymbol{\delta} \tag{4}$$

where $\langle \ldots \rangle$ represents an ensemble average and $\boldsymbol{\delta}$ is the unit tensor. In a BD simulation, we are rather interested in the numerical implementation of a multi-dimensional increment of a Wiener process $\Delta\mathbf{W}_{tt'} = (\mathbf{W})_t - (\mathbf{W})_{t'}$. Using the central limit theorem, it can be demonstrated that those increments are independent and follow also a Gaussian distribution with the next moments:

$$\langle (\mathbf{W})_t - (\mathbf{W})_{t'} \rangle = \mathbf{0} \tag{5}$$

$$\langle \big((\mathbf{W})_t - (\mathbf{W})_{t'}\big) \otimes \big((\mathbf{W})_t - (\mathbf{W})_{t'}\big) \rangle = |t - t'|\boldsymbol{\delta} \tag{6}$$

When implementing an explicit integration of a $\mathcal{D}$-dimensional Wiener process (defined in an orthogonal basis) in the time interval $[0, t_n]$, equi-partitioned in n intervals of size $\Delta t = t_i - t_{i-1}$, it is just necessary to define the initial value of the Wiener process, $(\mathbf{W})_0 = \mathbf{0}$, and calculate iteratively the increments as follows: $(\mathbf{W})_{t_i} = (\mathbf{W})_{t_{i-1}} + (\Delta\mathbf{W})_{t_i\, t_{i-1}}$, where each component of $\Delta\mathbf{W}_{t_i\, t_{i-1}}$ is obtained from an independent one-dimension normal distribution $\mathrm{N}(0, \Delta t)$.

Definition of the stochastic Brownian force given in (2) is coherent with the principle of equi-partition of energy, the fluctuation-dissipation theorem (in the sense that frictional force depends only on the instantaneous local velocity) and the formalisms of stochastic calculus [3].

Brownian dynamics is a limit case of the Langevin dynamics framework. In BD the inertial effects are neglected; in other words, BD supposes that no average acceleration takes place on the Brownian particle. In some physical sciences Brownian dynamics is also known as *overdamped* Langevin dynamics. Non-inertia assumption is justified in the insignificance of the inertial forces coming from small-mass particles in front of the viscous and thermal forces acting on the same particle. Brownian dynamics equation of motion for a Brownian particle writes therefore as follows:

$$\mathbf{0} = -\nabla U(\mathbf{r}) - \varsigma M\dot{\mathbf{r}} + \varsigma M\boldsymbol{\kappa}(\mathbf{r}) + \sqrt{2k_B T \varsigma M}\,\frac{d(\mathbf{W})_t}{dt} \tag{7}$$

Defining $\zeta = M\varsigma$ as the friction coefficient and $D = k_B T/\zeta$ as the diffusion coefficient of the particle, the instantaneous velocity of the Brownian particle can be written as follows:

$$\dot{\mathbf{r}} = \frac{-\nabla U(\mathbf{r})}{\zeta} + \boldsymbol{\kappa}(\mathbf{r}) + \sqrt{2D}\,\frac{d(\mathbf{W})_t}{dt} \tag{8}$$

Brownian dynamics simulations have been used intensively to study the physics of different kind of macromolecules and soft matter systems [4], as for example, the rheological behavior of polymer [5–10], the dynamics of proteins and DNA [11–14], the flow behavior of colloids [15–21], the structural dynamics of liquid-crystals [22, 23] and the dynamics of carbon nanotubes [24–27].

1.2 Rheology of Complex Fluids and Kinetic Theory

A comprehensive theoretical modelling of the problems in fluid dynamics requires a suitable formulation of the constitutive equation for the momentum flux or stress tensor. Flow of complex fluids differs from that one occurring in classical Newtonian fluids because it cannot be described by using a simple viscous constitutive equation. In fact, the mechanical response of a complex fluid to a given deformation appears to be viscoelastic, in other words, the complex fluid exhibits a mechanical behavior intermediate between perfect elastic solid and a perfect viscous liquid. Two viscoelastic regimes can be identified in function of the imposed strain. If the viscoelastic response is independent of the applied strain then we assist to the linear viscoelastic behavior. This mechanical regime is typically associated with very small deformations. On the other hand, when the viscoelastic response depends on the applied strain, then we deal with the non-linear viscoelastic regime. This paper is particularly focused on linear viscoelasticity because this mechanical regime constitutes the natural first approach in a rheological modelling framework.

The main aim of rheology consists to establish a suitable constitutive equation that relates stress and strain tensors for a given fluid and, sometimes, for a particular kind of flow. Kinetic theory in complex fluids is an exhaustive mathematical framework that looks for explaining the bulk flow phenomena based on the molecular structure of the fluid system. In that sense, kinetic theory is one of the tools employed by rheologists for generating suitable constitutive equations for non-Newtonian fluids. Formal framework in kinetic theory is built on coarse-grained representations of the molecular structure involved in the flow phenomena. Historically, the former coarse-grained molecular models appeared to emulate the polymer molecular structure. That explains why frequently the literature makes reference to *polymer* kinetic theory.

The coarse-grained molecular models in kinetic theory constitute a first attempt to relate the molecular structure to the bulk flow mechanics. Basic coarse-grained models emulate the most relevant characteristics of the molecular structure using beads, rods and springs as constitutive blocks. In what follows, an overview about the origins of bead-rod and the bead-spring models is illustrated based on the descriptions made by Bird et al. elsewhere [28].

1.2.1 Bead-Rod Model

Bead-rod models were proposed to emulate the structure of linear polymer chains. The first natural representation consisted in neglecting the pendant atoms or groups linked to the central chain and replacing this central chain by a series of beads and mass-less rods, where beads represent the constitutive atoms of the central chain and rods represent the chemical bonds between them. At this level of representation, the stochastic nature of the coarse-grained model emerges because all possible thermal interactions with the solvent molecules are reduced to an instantaneous stochastic

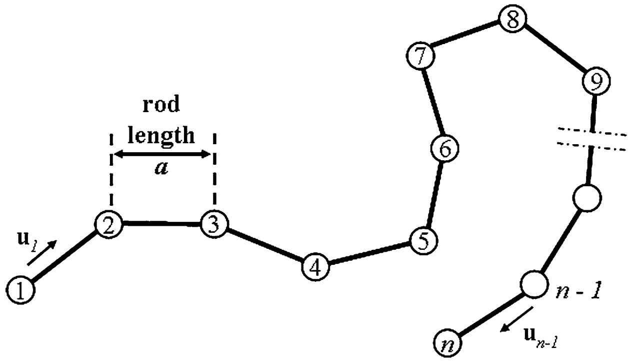

Fig. 1 Freely-jointed multi-bead-rod model composed of n beads and $n-1$ rods of length a

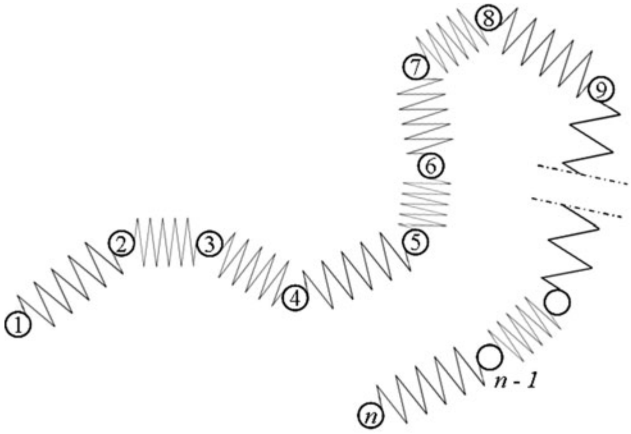

Fig. 2 Freely-jointed multi-bead-spring model composed of n beads and $n-1$ springs ($T > 0$ K)

force acting on each bead. Adjacent bonds in a linear polymer chain are restricted to very narrow intervals of solid angle values due to sterical hindering [29]. Based on this physical argument bead-rod chain model with fixed solid angles and restricted bond-rotation was proposed.

A simpler model considers that the rotational hindrances can be neglected, but the solid angles between adjacent rods are maintained. This representation is known as the *freely rotating chain model*. A complete series of articles about the non-equilibrium dynamics of the freely rotating chain model has been published before [30].

An even coarse-grained bead-rod model neglect any rotating and bending hindering between adjacent rods. This model is known as the *freely jointed multi-bead-rod* chain or, simply, *Kramers chain*. In this case, beads do not represent central chain atoms, but a portion of the polymer chain, typically 10–20 monomer units. In short, a Kramers chain can be described as an ensemble of n beads linked by $n-1$ rods of length a (see Fig. 1), where each bead is characterised by a drag coefficient ζ.

It has been demonstrated that supposing a random-walk distribution for the Kramers chain configuration the mean-square end-to-end distance of the chain at equilibrium writes (see for example [31]):

$$\langle r^2 \rangle_{eq} = a^2(n-1) \tag{9}$$

On the other hand, using a thermodynamic approach, it was shown that the average tension in a Kramers chain suspended in a solvent bath at temperature T and extended to a fixed end-to-end vector $\mathbf{r}$ (whose norm does not exceed one half of the contour length of the bead-rod chain) writes as follows [28]:

$$\mathbf{F}^{(c)}(\mathbf{r}) = \frac{3k_BT}{a^2(n-1)}\mathbf{r} \tag{10}$$

It is important to point out that previous expression is only exact when supposing a random-walk distribution for the configuration distribution function of the constitutive rods. In fact, this condition is only true for a large number of beads n [28]. It means that a 3-dimensional freely-jointed multi-bead-rod model behaves mechanically as a Hookean spring of null natural length with a spring constant H equals to:

$$H = \frac{3k_BT}{a^2(n-1)} = \frac{3k_BT}{\langle r^2 \rangle_{eq}} \tag{11}$$

1.2.2 Bead-Spring Model

Based on the characteristics of the mechanical behavior of a freely-jointed multi-bead-rod chain, it seemed natural to propose another up-level of coarse-graining for representing the structure of linear polymer chains. Actually, a linear polymer chain can be modelled as a series of springs, where each spring represents several hundreds of central chain atoms. Springs are linked by beads that concentrate masses and friction effects associated to the replaced central chain atoms. This model is called the freely-jointed multi-bead-spring chain (see Fig. 2). In principle, constitutive springs have null natural length, but simulations with non-zero natural length springs (e.g. Fraenkel-type) are also frequently employed. Several disadvantages appear at this level of coarse-graining; for instance, contour length is no more constant and, furthermore, if the spring potential is supposed Hookean, the chain can be infinitely extended, something that is physically unrealistic.

Considering a freely-jointed multi-bead-spring chain constituted of n beads linked by $n-1$ springs, it results not surprising that the average end-to-end distance at equilibrium be an extension of the analogue expression derived for the freely-jointed multi-bead-rod model:

$$\langle r^2 \rangle_{eq} = \frac{3k_BT(n-1)}{H} \tag{12}$$

In spite of the multi-bead-rod-spring models were initially developed in the framework of the *polymer* kinetic theory, those coarse-grained representations has been extended to model a vast kind of systems, including proteins, DNA, virus and carbon nanotubes. As mentioned before, this article will be focused on the BD simulation of the linear viscoelastic behavior of the bead-rod-spring models in absence of intermolecular interactions (hypothesis of infinitely diluted solution).

One can consider two different approaches when tackling with kinetic theory models in micro-to-macro simulations: a deterministic and a stochastic one. On the one hand, the deterministic approach deals with the direct solving of the FP equation at the expense of that the FP equation can be effectively formulated. FP or diffusion equation is a deterministic partial differential equation describing the evolution of the probability density function (in configurational space) of a given coarse-grained model. On the other hand, the stochastic approach proposes an extensive analysis of a representative population of coarse-grained models and the estimation of macroscopic properties by properly averaging the physical state of the population under consideration. Stochastic approach is conceivable for all coarse-grained kinetic theory models, even for those that do not have an equivalent FP equation. This paper presents the main issues of the latter approach by using a BD simulation tool for predicting the dynamic behavior of bead-rod-spring models in solution.

1.3 The Interest of the Stochastic Approach

A natural question that appears when dealing with flows of complex fluids is why to prefer using an extensive (and probably costly) method for integrating the FP diffusion equation of a given molecular model. An immediate answer to such question is simply that in some cases a FP diffusion equation is not available given the complexity of the coarse-grained model and, hence, the stochastic approach is the only method for accessing to the dynamic behavior of the molecular model.

On the other hand, in the classical framework of the kinetic theory, the equations of motion for the different constitutive blocks in a given coarse-grained model (beads, rods, springs) added to the continuity equation for the configurational distribution function can be used to build a FP diffusion equation. The common utility of this deterministic diffusion equation consists in recover the exact physical response of the system when submitted to a given external flow field by integrating the FP equation in the configurational space and in time (if looking for dynamic properties) in order to develop constitutive equations. Normally, those constitutive equations are employed a posteriori to calculate more complex flows by using a continuum mechanics framework. The crucial point in the previously described process lies on the mathematical method employed for integrating the diffusion equation given its multidimensional character. FP equation is a multidimensional function that depends on time and all the space coordinates chosen to define the configuration of the coarse-grained molecular model. It is necessary to point out that there is a vast collection of numerical strategies developed to solve this problematic integration [32–49].

However, it appears that the stochastic approach for solving the dynamics of coarse-grained models (even for those that have an equivalent FP diffusion equation) is employed more and more. In this case, we deal directly with the stochastic differential equation of motion for each coarse-grained system. In order to evaluate a given physical property, an average over a finite population of model systems has to be performed (in analogy to the integration of an equivalent FP equation in the configurational space). The main difficulties emerging with this approach are the associated stochastic noise, the low convergence order and the computational cost required to overcome the first two mentioned issues. Nevertheless, the growing-up leaning for tackling with the stochastic approach is due mainly to four reasons: (1) the dealing with complex coarse-grained structural descriptions that have not an equivalent FP formulation, (2) the enhanced possibility of enrich a given coarse-grained model by analyzing its configurational evolution under designed flow conditions, (3) the raising capacities of the computational tools that reduce simulation times, and (4) the interesting idea of resolving viscoelastic flow engineering problems without resorting to closed-forms of the constitutive equations for the stress tensor. This last idea means to establish micro-to-macro simulations where the configuration state of a population of coarsed-grained systems lets to calculate the stress field, allowing to compute the evolution of the flow field and, subsequently, to update the configurational space of coarse-grained models by solving the stochastic differential equations of motion [50–56].

Given the actual interest in the stochastic approach for solving the micro-to-macro modelling of viscoelastic flows, it is pertinent to review the fundamental numerical aspects associated with the solution of the differential stochastic equations for the simplest models in the kinetic theory framework. In that way, this paper analyses the main issues about the implementation of BD simulations for the bead-spring and bead-rod models. BD simulations in this paper are focused on predicting the dynamic response of dilute solutions of those coarse-grained kinetic theory models in the framework of linear viscoelasticity.

2 A Brownian Dynamics Algorithm for Simulating Linear Viscoelastic Behavior

From now on, an extensive Brownian dynamics modelling is systematically used to predict the dynamic response of a given bead-rod-spring chain model highly diluted within a Newtonian solvent. A classical rheological test used in linear viscoelasticity is simulated: a dynamic test of small-amplitude oscillatory deformation. Suspension is supposed confined between two parallel infinite-plates in the case of 3D simulations (see Fig. 3). In the case of 2D simulations, bead-rod-spring chain models are supposed confined in a plane xz of Fig. 3.

Oscillatory strain function is imposed by the relative sliding movement of the plates (or bars); inducing a homogeneous deformation within the suspension confined between the plates (or bars). Rheological response is supposed coming mainly from the bulk of the suspension, therefore wall and free-surface effects are ignored. Rheological properties are calculated from a properly defined average over N chain models, where N is the number of bead-rod-spring elements in the stochastic simulation. By the way, number of freedom degrees in the Brownian dynamics simulation is proportional to N. As suspension is supposed highly diluted, no interaction effects are considered between chain models and, hence, no computational storage of the relative positions between chains is necessary. A general flowchart of the algorithm intended to simulate a frequency sweep test in linear regime is presented in Fig. 4.

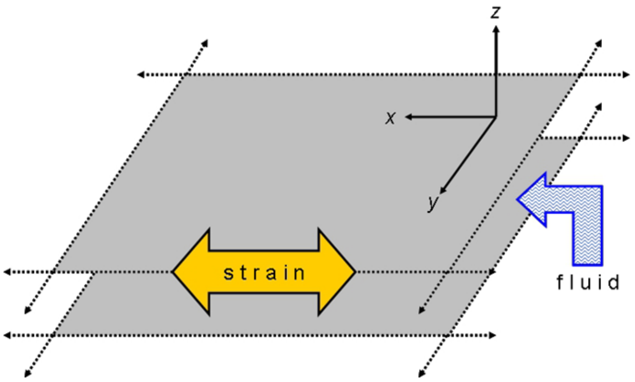

Fig. 3 Parallel infinite plates where BD simulations in shear rheology are carried out. *Upper plate* slides in relation to the *lower one* along the x axis for homogeneously shearing the fluid confined in between

The first step consists to obtain a configuration in thermal equilibrium. No external flow is imposed. Configuration of the BD system (N bead-rod-spring models) evolves in time under the action of the forces coming from the friction with the solvent, the internal energy potentials and the thermal interaction with the solvent molecules (Brownian effect). Time integration in this equilibrium stage is carried out until at least one of two criteria is satisfied: stabilization of the stored internal energy (when it can be estimated) or integration during at least three times the longest characteristic time associated with an equivalent bead-rod-spring chain whose FP equation has an analytical solution. For instance, as internal energy is not accessible for freely-jointed bead-rod models, equilibrium step is carried out during three times the rotational time of an equivalent multi-bead rigid-rod with the same length.

Fig. 4 Flowchart of the general BD algorithm for simulating a small-amplitude oscillatory deformation test

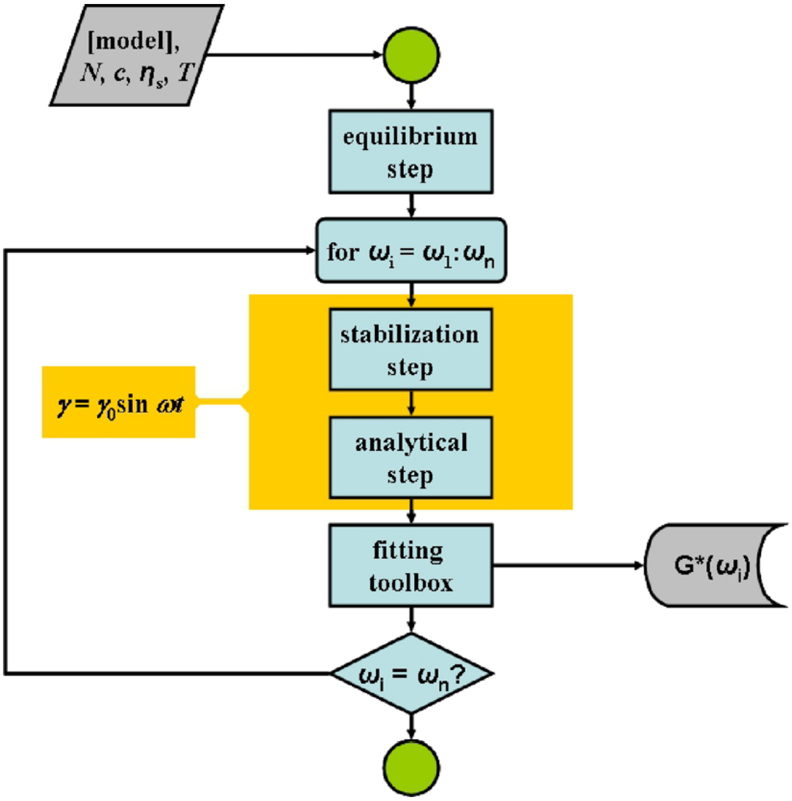
[model], N, c, η_s, T
equilibrium step
for $\omega_i = \omega_1 : \omega_n$
stabilization step
analytical step
$\gamma = \gamma_0 \sin \omega t$
fitting toolbox
$G^*(\omega_i)$
$\omega_i = \omega_n$?

Once the equilibrium configuration of the BD system has been obtained, the dynamic strain function $\gamma = \gamma_0 \sin \omega t$ can be applied, where γ_0 is a deformation within the linear regime. Frequency sweep test is carried out on a finite number of frequencies homogeneously distributed in logarithmic scale between the lowest frequency ω_1 and the highest frequency ω_n. The BD prediction of the complex modulus at each tested frequency is composed of two steps. First, a dynamic stabilisation of the BD system is carried out either until internal energy dynamic stabilization or during at least three times the longest characteristic time of an equivalent bead-rod-spring model before starting the second stage, called analytical step, in which the BD-calculated shear-stress signal is stored during one-and-a-half periodic oscillations. This signal is used as entry variable in a fitting toolbox with the aim to determine the parameters (τ_0, δ) of a smooth shear-stress function $\tau = \tau_0 \sin(\omega t + \delta)$ by using a Newton-based error-minimization methodology. Dynamic complex modulus at each frequency is then computed easily in the next way:

$$G^*(\omega) = G'(\omega) + i G''(\omega) = \frac{\tau_0}{\gamma_0} \cos \delta + i \frac{\tau_0}{\gamma_0} \sin \delta \tag{13}$$

where G' is the storage modulus and G'' is the loss modulus.

3 BD of Generalized Bead-Spring Models

Even though the multi-bead-rod model appeared chronologically earlier than the multi-bead-spring model, this latter is tackled preliminarily here because it offers a simpler mathematical structure that is reflected on the simplicity of the BD numerical methods associated with. In addition, due probably to the simpler mathematic formalisms, the multi-spring-bead model has been more recurrently employed to model the dynamics of complex fluids.

3.1 Kinematic and Dynamic Formulation

Let consider the multi-bead-spring chain model in Fig. 2. In what follows, a multi-bead-spring chain is constituted of n beads joined by $n - 1$ non-bendable springs. The instantaneous position of each bead is defined in a coordinate reference system by the vector $\mathbf{r}_i$. An alternative way for describing the position and the orientation of the multi-bead-spring chain is possible defining the center of masses of the chain, $\mathbf{r}_c$ and the connector vector $\mathbf{Q}_i$ between consecutive beads:

$$\mathbf{r}_c = \frac{1}{n} \sum_{i=1}^{n} \mathbf{r}_i \tag{14}$$

$$\mathbf{Q}_i = \mathbf{r}_{i+1} - \mathbf{r}_i \tag{15}$$

Multi-bead-spring chain is supposed suspended into a solvent at temperature T. Solvent is considered a Newtonian fluid with viscosity η_s. Concentration of the multi-bead-spring chains is defined in terms of the density of chains, c chains per volume unit. As the solution is supposed highly diluted no interaction between multi-bead-spring chains is considered. Moreover, flow field in the overall suspension is supposed homogeneous, in the meaning that the rate-of-strain tensor is the same in all points of the flow field or, at least, in the scale of twice the contour length of the multi-bead-spring chain [28].

In the kinematic formulation of this kind of coarse-grained model is presumed that all changes of momentum are concentrated on beads. Furthermore, an assumption of inertia-less is employed; due to the insignificance of inertial forces (small masses) with respect to friction and thermal forces acting on them. In what follows a detailed description of the forces acting on beads is presented.

- Hydrodynamic drag force acting on bead i, $\mathbf{F}_i^{(h)}$

  This force describes the resistance experienced by the bead as it moves through the fluid. One of the simplest ways to express this force is given by the Stoke's law, which considers the hydrodynamic drag force proportional to the difference between the fluid velocity at the bead position and the averaged bead velocity. A more general expression takes into account a hydrodynamic interaction component that comes from the physical perturbation of the local flow field due to the global chain movement. Hydrodynamic drag force acting on bead i writes as follows:

$$\mathbf{F}_i^{(h)} = \boldsymbol{\zeta} \left(\boldsymbol{\kappa}(\mathbf{r}_i) \cdot \mathbf{r}_i + \mathbf{v}'_i - \dot{\mathbf{r}}_i \right) \tag{16}$$

  where $\boldsymbol{\zeta}$ is a second-order friction tensor, $\boldsymbol{\kappa}$ is the gradient of the bulk velocity field and $\dot{\mathbf{r}}_i$ is the averaged instantaneous bead velocity. On the other hand, $\mathbf{v}'_i$ accounts for the variation in the local flow field around $\mathbf{r}_i$ due to the motion of the other beads in the same chain.

  In *polymer* kinetic theory, Rouse model neglects this intra-molecular interaction (i.e. $\mathbf{v}'_i = \mathbf{0}$); resorting to the well-known *free draining motion* hypothesis [57]. On the other hand, theories taking into account the hydrodynamic interaction suppose that the bead velocity $\mathbf{v}'_i$ depends linearly on the hydrodynamic forces acting on the others beads inside the chain:

$$\mathbf{v}'_i = - \sum_j \boldsymbol{\Omega}_{ij} \cdot \mathbf{F}_j^{(h)} \tag{17}$$

  where $\boldsymbol{\Omega}_{ij}$ is the Oseen-Burgers hydrodynamic interaction tensor associated with a given pair of beads i and j. Say that the perturbation of a velocity field in a given point of the space depends linearly on the hydrodynamic forces acting in the surroundings of that point presupposes a Maxwellian velocity distribution [28]. Oseen-

Burgers hydrodynamic tensor writes as follows:

$$\boldsymbol{\Omega}_{ij} = \frac{1}{8\pi\eta_s r_{ji}}\left(\boldsymbol{\delta} + \frac{\mathbf{r}_{ji}\otimes\mathbf{r}_{ji}}{r_{ji}^2}\right) \quad \text{for } i \neq j \tag{18}$$

where $\mathbf{r}_{ji} = \mathbf{r}_i - \mathbf{r}_j$ and $r_{ji} = \|\mathbf{r}_{ji}\|$. On the other hand, $\boldsymbol{\Omega}_{ii} = \mathbf{0}$. Zimm model, in the context of *polymer* kinetic theory, takes into account the hydrodynamic interaction effect using the equilibrium-averaged Oseen-Burgers tensor [58]:

$$\langle\boldsymbol{\Omega}_{ij}\rangle_{eq} = \frac{1-\delta_{ij}}{6\pi\eta_s}\left\langle\frac{1}{r_{ji}}\right\rangle_{eq}\boldsymbol{\delta} \quad \text{for } i \neq j \tag{19}$$

where δ_{ij} is the *Kronecker delta*.

- Intra-molecular force acting on bead i, $\mathbf{F}_i^{(\phi)}$

  This force corresponds to the sum of all the spring forces acting on bead i. In a multi-bead-spring chain, total intra-molecular force on bead i writes as follows:

$$\mathbf{F}_i^{(\phi)} = \sum_{j=1}^{n-1}(\delta_{ij} - \delta_{i\,j+1})\mathbf{F}_j^{(c)} \tag{20}$$

where $\mathbf{F}_j^{(c)} = \partial\phi_j/\partial\mathbf{Q}_j$ is the connector force acting on bead j along spring j, defined as the gradient of the spring potential energy ϕ_j. Linear force law is the simplest connector force:

$$\mathbf{F}_i^{(H)} = \frac{\partial\phi_i^{(\mathrm{LIN})}}{\partial\mathbf{Q}_i} = \frac{\partial}{\partial\mathbf{Q}_i}\left(\frac{1}{2}H(\sqrt{\mathbf{Q}_i\cdot\mathbf{Q}_i})^2\right) = H\mathbf{Q}_i \tag{21}$$

Previous Hookean-type law force is based on the entropic analysis over a tighten random-walk polymer chain. H is a Hookean spring constant that can be related to temperature and some molecular structural parameters (see Sect. 1.2.1). The linear law force is only valid for large polymer chains and small strain regimes. Hence, Hookean law force is inadequate for processes involving large deformations. This fact motivated the use of non-linear force laws, for instance:

- Finite extensible non-linear elastic (FENE) force law [59]

$$\mathbf{F}_i^{(\mathrm{FENE})} = \frac{H\mathbf{Q}_i}{1-(Q_i/Q_{i,0})^2} \tag{22}$$

  where $Q_i = \|\mathbf{Q}_i\|$ and $Q_{i,0}$ is the maximal extension of the spring.

- Inverse Langevin (IL) force law [60]

$$\mathbf{F}_i^{(\mathrm{IL})} = \frac{k_B T}{a'}\mathcal{L}^{-1}\left[\frac{\mathbf{Q}_i}{Q_{i,0}}\right] \tag{23}$$

  where a' is typically twice the persistence length l_p and the Langevin function $\mathcal{L}$ is given by $\mathcal{L}(x) = \coth(x) - x^{-1}$. Persistence length in a polymer molecule is a measure of the flexibility of the chain; in other terms, the direction of the chain-axis in a quiescent polymer molecule is uncorrelated only along contour length distances equal or higher than $2l_p$.

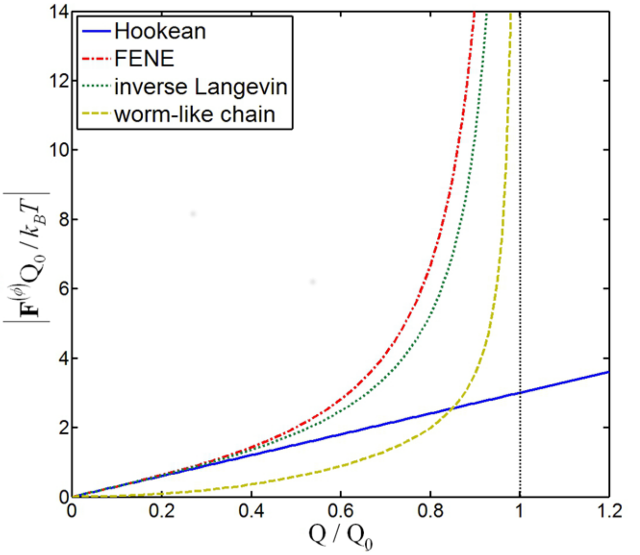

Fig. 5 Curves of the spring connector force $|\mathbf{F}^{(\phi)}|$ in function of the reduced spring extension for several spring force laws employed in *polymer* kinetic theory

- Worm-like chain (WLC) force law [61]

$$\mathbf{F}_i^{(\mathrm{WLC})} = \frac{k_B T}{a'}\left[\frac{1}{2}\frac{1}{(1-Q_i/Q_{i,0})^2} - \frac{1}{2} + \frac{2Q_i}{Q_{i,0}}\right] \times \frac{\mathbf{Q}_i}{Q_{i,0}} \tag{24}$$

A comparison of the various spring-force laws is presented in Fig. 5. Observe that FENE-like force laws are linear at small extensions and tends to infinite when extension approaches the finite maximal length.

- Brownian force acting on bead i, $\mathbf{F}_i^{(b)}$

  The Brownian force accounts for the change of momentum at each bead (supposed as Brownian particles) due to the ensemble of instantaneous collisions of the solvent molecules against it. In nature, those collisions are faster than the bead motion, that is why Brownian forces are considered as stochastic variables in the BD time scale. Due to the isotropic condition of those collisions, Brownian force is treated mathematically as a quantity with zero mean in time and space (ergodicity principle). On the other hand, the second-moment of the distribution of Brownian forces must equilibrate the dissipative forces [3]. In short, an "instantaneous" Brownian force distribution in a BD simulation is characterised as a Gaussian process with the next first and second moments:

$$\left\langle\mathbf{F}_i^{(b)}(t)\right\rangle = \mathbf{0} \tag{25}$$

$$\left\langle \mathbf{F}_i^{(b)}(t) \otimes \mathbf{F}_j^{(b)}(t+\Delta t) \right\rangle = \frac{2k_B T}{\Delta t} \boldsymbol{\zeta} \tag{26}$$

where Δt is a discrete approximation of a differential in time. It is important to mention that in an orthogonal basis ($\mathcal{D}$ dimensions) the multi-dimensional Gaussian process can be decoupled in $\mathcal{D}$ independent uni-dimensional Gaussian processes [3].

- External forces acting on bead i, $\mathbf{F}_i^{(e)}$
  Gravitational and electromagnetic fields can induce non-negligible external forces over the beads of the system. Nevertheless, these forces are not considered here.

Taking into account that beads are considered as Brownian particles, the inertial effects are neglected. In such context, the force balance must to be satisfied at each time and at each bead i:

$$\mathbf{F}_i^{(h)} + \mathbf{F}_i^{(\phi)} + \mathbf{F}_i^{(b)} + \mathbf{F}_i^{(e)} = \mathbf{0} \tag{27}$$

Using the definition of the hydrodynamic drag force, previous differential stochastic equation can be transformed to explicit the bead velocity:

$$\frac{d\mathbf{r}_i}{dt} = \mathbf{v}_i' + \left[\boldsymbol{\kappa}(\mathbf{r}_i) \cdot \mathbf{r}_i\right] + \boldsymbol{\zeta}^{-1}\mathbf{F}_i^{(\phi)} + \boldsymbol{\zeta}^{-1}\mathbf{F}_i^{(b)} + \boldsymbol{\zeta}^{-1}\mathbf{F}_i^{(e)} \tag{28}$$

Integration in time of previous stochastic equation governs the kinematic evolution of the bead-spring system. As any numerical method, in a BD simulation time is treated as a discrete variable and, hence, different numerical integration schemes can be proposed.

3.2 Integration Schemes

Given the structure of Eq. (28) a simple explicit integration scheme inspired by the numerical resolution of ordinary differential equations appears as a natural integration scheme. In fact, the Euler-Maruyama method is the simplest way to integrate numerically Eq. (28). Given an initial configuration at time t, $(\mathbf{r}_i)_t$, it is possible to estimate $(\mathbf{r}_i)_{t+\Delta t}$ by using the next formula:

$$(\mathbf{r}_i)_{t+\Delta t} = (\mathbf{r}_i)_t + \left(\mathbf{v}_i' + \left[\boldsymbol{\kappa}(\mathbf{r}_i) \cdot \mathbf{r}_i\right] + \boldsymbol{\zeta}^{-1}\mathbf{F}_i^{(\phi)}\right)_t \Delta t + \left(\sqrt{2k_B T \boldsymbol{\zeta}^{-1}}\right)\Delta \mathbf{W}_i \tag{29}$$

where $\Delta\mathbf{W}$ is a random increment following a multi-dimensional Wiener process. This random Wiener process follows a normal distribution with the next first and second moments:

$$\langle \Delta \mathbf{W}_i \rangle = \mathbf{0} \tag{30}$$

$$\left\langle (\Delta \mathbf{W}_i)_t \otimes (\Delta \mathbf{W}_j)_{t+\Delta t} \right\rangle = \Delta t \boldsymbol{\delta} \tag{31}$$

Rewriting Eq. (29) only in terms of the time step Δt we have:

$$(\mathbf{r}_i)_{t+\Delta t} = (\mathbf{r}_i)_t + \left(\mathbf{v}_i' + \left[\boldsymbol{\kappa}(\mathbf{r}_i) \cdot \mathbf{r}_i\right] + \boldsymbol{\zeta}^{-1}\mathbf{F}_i^{(\phi)}\right)_t \Delta t + \left(\sqrt{2k_B T \boldsymbol{\zeta}^{-1}\Delta t}\right)\Delta \mathbf{N}_i(0,1) \tag{32}$$

where $\Delta\mathbf{N}_i(0,1)$ is a multi-dimensional Gaussian increment of mean 0 and variance 1. Performance of the Euler-Maruyama method is extremely sensitive to the time step employed. In fact, convergence of the integration scheme is only guaranteed when $\Delta t \to 0$ [62]. Suppose a stochastic differential equation with the next general form:

$$dX = A(X)\,dt + B(X)\,dW \tag{33}$$

An integration scheme converges strongly with order υ at time $t_{\max}$ if the next condition is satisfied:

$$\left\langle \left| X(t_{\max}) - X_{\text{true}}(t_{\max}) \right|^2 \right\rangle^{1/2} \leq C(\Delta t)^{\upsilon} \tag{34}$$

for all time step lengths equal or inferior to Δt and C being a positive constant. It has been proven that the Euler-Maruyama method exhibit a low order of strong convergence $\upsilon = 1/2$ [3]. Identification of the maximal time step satisfying the strong convergence criteria for a specific C value is normally done by trial and error and plotting the error in function of the time step. In spite of the low order of convergence, when the drift and diffusive coefficients ($A(X)$ and $B(X)$ in Eq. (33) respectively) are almost constants, the Euler-Maruyama method is the most frequently used integration scheme. Thus, this explicit integration scheme is widely used in BD simulations for bead-spring systems with Hookean-springs.

Now, when the drift and diffusion coefficients become more complex, the fully explicit method is not satisfying and high order integration schemes are required. Such is the case when non-linear spring potentials are employed to guarantee a finite spring extensibility. In fact, the main difficulty appearing with the numerical temporal integration of this kind of bead-spring systems is that the bead displacements have to be bounded in order to not exceed the maximal spring extension. For describing those high-order integration algorithms is better to express the bead-spring chain dynamics (given in Eq. (28)) in terms of the connector vector $\mathbf{Q}_i$:

$$\frac{d\mathbf{Q}_i}{dt} = \left(\mathbf{v}_{i+1}' - \mathbf{v}_i'\right) + \left[\boldsymbol{\kappa}(\mathbf{r}_i) \cdot \mathbf{Q}_i\right] + \boldsymbol{\zeta}^{-1}\left(\mathbf{F}_{i+1}^{(\phi)} - \mathbf{F}_i^{(\phi)}\right) + \boldsymbol{\zeta}^{-1}\left(\mathbf{F}_{i+1}^{(b)} - \mathbf{F}_i^{(b)}\right) \tag{35}$$

A first approximation to solve the previous equation containing non-linear spring forces consists in use a conventional explicit scheme (Euler-Maruyama method) and just reject the updating step that produces a not-physical displacement (maximal spring extension exceeded). Some practical rejection criteria and useful advices for the choice of the time step are given elsewhere [3].

More appropriate methods to integrate Eq. (35) are based on implicit schemes. For example, Somasi et al. [63] proposed a fully implicit scheme inspired in the two-step semi-implicit algorithm proposed by Öttinger for FENE dumbbells [3]. In general, at each time step, those implicit methods are composed of a predictor step followed by a corrector one. Given a bead-spring configuration at the time t, $(\mathbf{Q}_i)_t$, the configuration after one time step is generated as follows:

- *Predictor step*. Using a conventional explicit scheme a test configuration $\mathbf{Q}_i^*$ is calculated as follows:

$$\mathbf{Q}_i^* = (\mathbf{Q}_i)_t + \Big[\big(\mathbf{v}'_{i+1} - \mathbf{v}'_i\big)_t + \big[\boldsymbol{\kappa}(\mathbf{r}_i) \cdot (\mathbf{Q}_i)_t\big] \\ + \boldsymbol{\zeta}^{-1}\big(\mathbf{F}_{i+1}^{(\phi)} - \mathbf{F}_i^{(\phi)}\big)_t + \boldsymbol{\zeta}^{-1}\big(\mathbf{F}_{i+1}^{(b)} - \mathbf{F}_i^{(b)}\big)_t\Big]\Delta t \tag{36}$$

- *Corrector step*. Rewriting the spring potential forces in terms of the connector forces (Eq. (20)) and using the test configuration obtained in the predictor step to average the flow-field contribution to the drag forces is possible to write a corrector step as follows:

$$\begin{aligned} &\overline{\mathbf{Q}}_i + 2\boldsymbol{\zeta}^{-1}\overline{\mathbf{F}}_i^{(c)}\Delta t \\ &\quad = (\mathbf{Q}_i)_t + \frac{1}{2}\big[\boldsymbol{\kappa}(\mathbf{r}_i) \cdot (\mathbf{Q}_i)_t + \boldsymbol{\kappa}(\mathbf{r}_i) \cdot \mathbf{Q}_i^*\big]\Delta t \\ &\qquad + \boldsymbol{\zeta}^{-1}\big(\overline{\mathbf{F}}_{i-1}^{(c)} + \big(\mathbf{F}_{i+1}^{(c)}\big)_t\big)\Delta t \\ &\qquad + \boldsymbol{\zeta}^{-1}\big(\mathbf{F}_{i+1}^{(b)} - \mathbf{F}_i^{(b)}\big)_t\Delta t \end{aligned} \tag{37}$$

  where spring forces for connectors i and $i-1$ are treated implicitly when solving for $\overline{\mathbf{Q}}_i$. Rearrangement of Eq. (37) generates a cubic equation for the magnitude of $\overline{\mathbf{Q}}_i$, whose unique root is inferior to the maximal spring extensibility. In the final stage of the corrector step, spring force of the connector $i+1$ is given by Eq. (37) and spring forces for connectors i and $i-1$ are tackled implicitly again:

$$\begin{aligned} &\overline{\mathbf{Q}}_i^{[n]} + 2\boldsymbol{\zeta}^{-1}\big(\overline{\mathbf{F}}_i^{(c)}\big)^{[n]}\Delta t \\ &\quad = (\mathbf{Q}_i)_t + \frac{1}{2}\big[\boldsymbol{\kappa}(\mathbf{r}_i) \cdot (\mathbf{Q}_i)_t + \boldsymbol{\kappa}(\mathbf{r}_i) \cdot \overline{\mathbf{Q}}_i^{[n-1]}\big]\Delta t \\ &\qquad + \boldsymbol{\zeta}^{-1}\big(\big(\overline{\mathbf{F}}_{i-1}^{(c)}\big)^{[n]} + \mathbf{F}_{i+1}^{(c)}\big)\Delta t \\ &\qquad + \boldsymbol{\zeta}^{-1}\big(\mathbf{F}_{i+1}^{(b)} - \mathbf{F}_i^{(b)}\big)_t\Delta t \end{aligned} \tag{38}$$

  Previous equation gives also a cubic equation for the nth approximation of $\overline{\mathbf{Q}}_i^{[n]}$ and, hence, an iterative process can be formulated (doing $\overline{\mathbf{Q}}_i^{[n-1]}$ equal to $\overline{\mathbf{Q}}_i^{[n]}$) until difference between consecutive solutions is inferior to a specified tolerance ε:

$$\sqrt{\sum_{i=1}^{n-1}\big(\overline{\mathbf{Q}}_i^{[n]} - \overline{\mathbf{Q}}_i^{[n-1]}\big)^2} \leq \varepsilon \tag{39}$$

  Once the iterative process converges, $\overline{\mathbf{Q}}_i^{[n]}$ is said to be the spring configuration at time $t + \Delta t$, $(\mathbf{Q}_i)_{t+\Delta t}$, with the guarantee that the lengths of the connector vectors are allowed physical ones.

In spite of the heavier calculus involved at each time step in relation to the explicit algorithm, the advantage of the implicit schemes is that larger time steps can be employed. For such reason, each modelling requires a particular analysis for determining which integration method produces a more efficient BD simulation.

Several studies about the numerical integration of non-linear stochastic equations and time step width control are found elsewhere, as well as, relevant examples of BD simulations of bead-spring systems with finite-extensibility spring potentials [64–66].

3.3 Stress Tensor Calculation

In order to obtain the rheological behavior of any coarse-grained molecular model it is necessary to extract the stress tensor information from its mechanical balance at each instant. Total shear-stress tensor $\boldsymbol{\tau}$ in a suspension is supposed to be the sum of the contribution coming from the solvent $\boldsymbol{\tau}_s$ and another one coming from the suspended entities $\boldsymbol{\tau}_p$ (in this case, the multi-bead-spring chains) [28]:

$$\boldsymbol{\tau} = \boldsymbol{\tau}_s + \boldsymbol{\tau}_p \tag{40}$$

It is important to notice that at equilibrium (i.e. no external forces and no external-flow field), the total shear stress tensor $\boldsymbol{\tau}$ is zero. Assuming that the solvent is a Newtonian fluid, then previous Eq. (40) can be rewritten as follows:

$$\boldsymbol{\tau} = \eta_s\dot{\boldsymbol{\gamma}} + \boldsymbol{\tau}_p \tag{41}$$

where η_s is the solvent viscosity and $\dot{\boldsymbol{\gamma}}$ is the homogeneous rate-of-strain tensor. Anyway, to model the intrinsic rheological response of the bead-spring chain, one is particularly interested on the shear stress contribution coming from the suspended particles $\boldsymbol{\tau}_p$. In the early literature of *polymer* kinetic theory there are several formal derivations of expressions accounting for the shear stress tensor contribution coming from multi-bead-spring chains suspended in liquid media [67, 68]. According to those developments in a bead-spring chain there are three principal physical effects contributing to the total shear stress tensor: (1) the intramolecular forces across the connector vectors; (2) the external forces acting on beads and (3) the transport of momentum caused by the displacement of the beads. Those are not the only sources contributing to the physical mechanical state of the system, but in the framework of a standard rheological test those described mechanisms are definitively the most important.

Based on this deduction guideline, the Kramers expression for the shear-stress tensor contribution coming from a multi-bead-spring chain writes as follows:

$$\boldsymbol{\tau}_p = c\sum_{k=1}^{n-1}\left\langle \mathbf{Q}_k \otimes \mathbf{F}_k^{(c)}\right\rangle - c\sum_{v=1}^{n}\sum_{k=1}^{n-1} B_{vk}\left\langle \mathbf{Q}_k \otimes \mathbf{F}_v^{(e)}\right\rangle - (n-1)ck_B T\boldsymbol{\delta} \tag{42}$$

where B_{vk} is a scalar operator associated with bead v and spring k given by [28]:

$$B_{vk} = \begin{cases} \frac{k}{n} & k < n \\ -[1-\frac{k}{n}] & k \geq n \end{cases} \tag{43}$$

In fact, the configuration of a bead-spring chain can be specified alternatively by the position of the center of mass of the chain $\mathbf{r}_c$ and the $n-1$ connector vectors $\mathbf{Q}_k$ as follows:

$$\mathbf{r}_v = \mathbf{r}_c + \sum_{k=1}^{n-1} B_{vk}\mathbf{Q}_k \tag{44}$$

In the right side of Kramers expression in Eq. (42) are easily identifiable the three mentioned physical effects contributing to the shear-stress tensor: the first term corresponds to the intra-molecular forces contribution, the second one represents the contribution of the external forces and the third one accounts for the momentum transfer of beads (Brownian contribution). This last term is an isotropic contribution to the shear stress tensor based on the supposition of a Maxwellian velocity distribution.

Kramers expression can be slightly transformed by writing the spring-bead chain conformation in terms of the distance of each bead to the center of mass of the chain, $\mathbf{R}_v = \mathbf{r}_v - \mathbf{r}_c$, and by using the expression relating the intra-molecular force acting on bead v, $\mathbf{F}_v^{(\phi)}$, with the connector force $\mathbf{F}_k^{(c)}$ associated to spring k (Eq. (20)). Such form is known as the modified-Kramers expression for the shear-stress tensor contribution of a bead-spring chain:

$$\boldsymbol{\tau}_p = -c\sum_{v=1}^{n}\left\langle \mathbf{R}_v \otimes \left(\mathbf{F}_v^{(\phi)} + \mathbf{F}_v^{(e)}\right)\right\rangle - (n-1)ck_B T\boldsymbol{\delta} \tag{45}$$

Now, combining previous equation with the bead force balance in a multi-bead-spring chain given in Eq. (27) and neglecting any external force a much simpler expression for the shear stress tensor can be obtained:

$$\boldsymbol{\tau}_p = c\sum_{v=1}^{n}\left\langle \mathbf{R}_v \otimes \mathbf{F}_v^{(h)}\right\rangle \tag{46}$$

where the result,

$$\sum_{v=1}^{n}\left\langle \mathbf{R}_v \otimes \mathbf{F}_v^{(b)}\right\rangle = (n-1)k_B T\boldsymbol{\delta} \tag{47}$$

has been employed supposing again a Maxwellian velocity distribution. Shear-stress tensor contribution in Eq. (46) is known as the Kramers-Kirkwood expression [30, 67].

Non intuitively, BD simulations with bead-spring models in 2D and 3D produced the same results. In what follows of the current Sect. 3, only the predictions in 3D are given.

3.4 The Rouse Model

Rouse model is a *polymer* kinetic theory model that mimics the structure of a linear polymer chain using a multi-bead-spring chain, where intra-molecular interactions are neglected. Springs in the Rouse model follows a Hookean law, based on the results of the end-to-end entropic tension experimented by a freely-jointed Kramers chain (following a Gaussian distribution configuration) suspended in an isothermal solvent bath (see Sect. 1.2.1). No external forces are considered. A formal compendium of the theory can be found in the recognized publication of Rouse in 1953 [57].

3.4.1 The Hookean-Dumbbell

The simplest version of the Rouse model is the (two-beads)–(one-spring) system or, better known as, the elastic-dumbbell model. It has been found that the mechanical response of the dumbbell model is equivalent to that one of a Maxwell element (spring-dashpot in series) used by rheologists to model a general linear viscoelastic behavior [69].

Given the simplicity of the dumbbell model, it will be used to study the main numerical issues of the BD simulations for bead-spring models. An explicit integration scheme has been employed in a three-dimensional BD simulation. In what follows, the equilibrium properties and dynamical behavior are analysed in detail.

Equilibrium Properties A (two-beads)–(Hookean-spring) system at thermal equilibrium and in absence of an external-flow field has an average square end-to-end distance $\langle r^2\rangle_{eq}$ equal to:

$$\left\langle r^2\right\rangle_{eq} = \frac{3k_B T}{H} \tag{48}$$

An important aspect in BD simulations is the number of entities (or trajectories) required to converge to the central

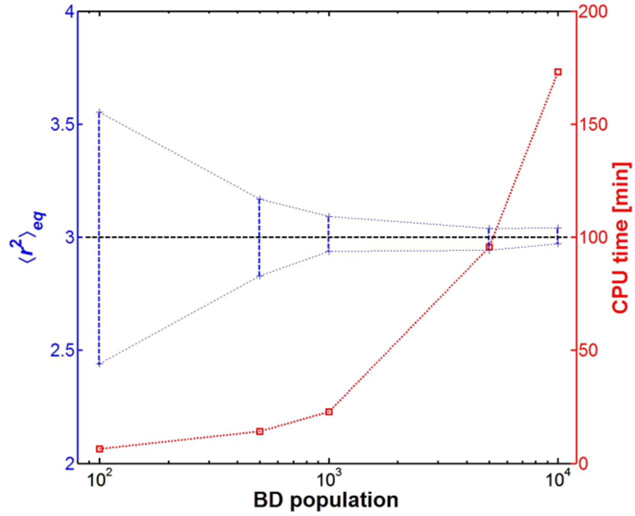

Fig. 6 Statistics of the square end-to-end distance of a Hookean dumbbell in thermal equilibrium (during 1500 time steps) in function of the BD population. H, ζ and ck_BT are fixed to 1 in a consistent system of units. Square end-to-end distance at equilibrium is equal to 3 according to the kinetic theory. A time step equal to $\lambda_H/250$ has been employed

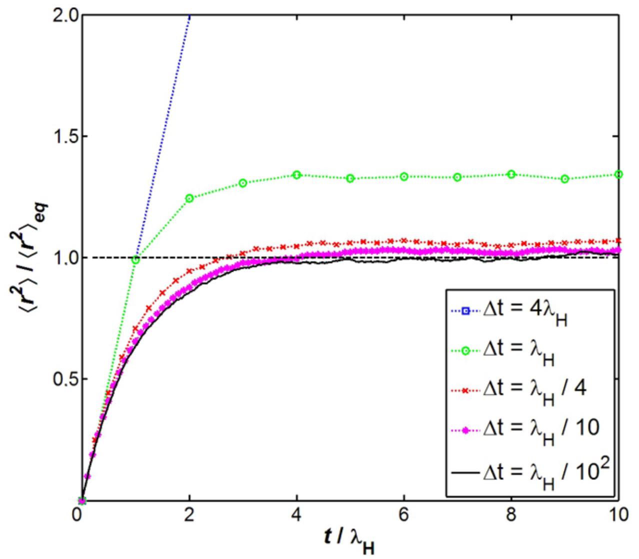

Fig. 7 Evolution of the reduced square end-to-end distance of a dumbbell after sudden thermal activation for different time steps in the BD simulation. H, ζ and ck_BT are fixed to 1 in a consistent system of units. Square end-to-end distance is made dimensionless using the equilibrium value given by the kinetic theory. A population of 10^4 dumbbells has been employed

values with satisfactory statistics. In Fig. 6 the BD performance to estimate the square end-to-end distance in function of the population considered is presented.

The simulated Hookean dumbbell has a square end-to-end distance at equilibrium equal to 3 (given by Eq. (48)) and a relaxation time of $\lambda_H = 0.25$ according to the kinetic theory framework. A short time step ($\Delta t = \lambda_H/250$) was employed in the simulation in order to marginalize the effect of the integration scheme convergence. BD performance is measured as the dispersion of the average square end-to-end distance (95 % of confidence) for 1500 time steps once the system has reached an equilibrium configuration (i.e. after at least 3 times the relaxation time). A reduction of the relative dispersion with respect to the central value is observed from 18.5 % for a population of 10^2 dumbbells to 1.1 % for a population of 10^4 dumbbells. As expected, a linear evolution of the computational time (Intel® Core™ T7300 2.00 GHz) in function of the number of dumbbells simulated is noticed. For this particular case, a good compromise between simulation accuracy and computational time is obtained for populations between of 10^3 and 5×10^3 dumbbells.

Another important issue in BD simulations, especially when employing an explicit integration scheme, is time step. In Fig. 7 the influence of the time step on the convergence of the integration scheme is revealed. In this case a population of 10^4 dumbbells is employed with the aim to attenuate the noise coming from the random number generation of statistical distributions and isolate the effects originated by the integration scheme.

In Fig. 7 the evolution of the squared end-to-end distance of a Hookean dumbbell, after a sudden thermal activation, is presented for different time steps. In absence of temperature, the end-to-end distance of a dumbbell is null. That is the reason why all curves begin at the origin. According to the kinetic theory, a time equal to four times the relaxation time is more than enough for a Hookean dumbbell model to reach the equilibrium end-to-end distance at constant temperature. From Fig. 7, a complete divergence of the integration scheme is observed when a time step bigger than the main relaxation time is employed. For a time step equal to the relaxation time and equal to a quarter of the relaxation, the integration scheme does not diverge, but the steady values are inaccurate regarding the exact solution. On the other hand, a finer convergence towards the central values is observed as the time step gets smaller than a tenth of the relaxation time.

At thermal equilibrium the shear-stress tensor is zero, so for a Hookean dumbbell Kramers expression (Eq. (42)) writes:

$$\boldsymbol{\tau}_{p,\,eq} = c\left\langle \mathbf{Q} \otimes \mathbf{F}^{(c)} \right\rangle - ck_BT\boldsymbol{\delta} = \mathbf{0} \tag{49}$$

which could be written also as:

$$\frac{\langle \mathbf{Q} \otimes \mathbf{F}^{(c)} \rangle_{eq}}{k_BT} = \boldsymbol{\delta} \tag{50}$$

Using a time step equal to $\lambda_H/100$ and an equilibrated population of 10^3 dumbbells (i.e. a BD system equilibrated during a time equal to three times the main relaxation time), the simulation produces a stable shear stress tensor. Third of the trace of the tensor in the left member of Eq. (50) has

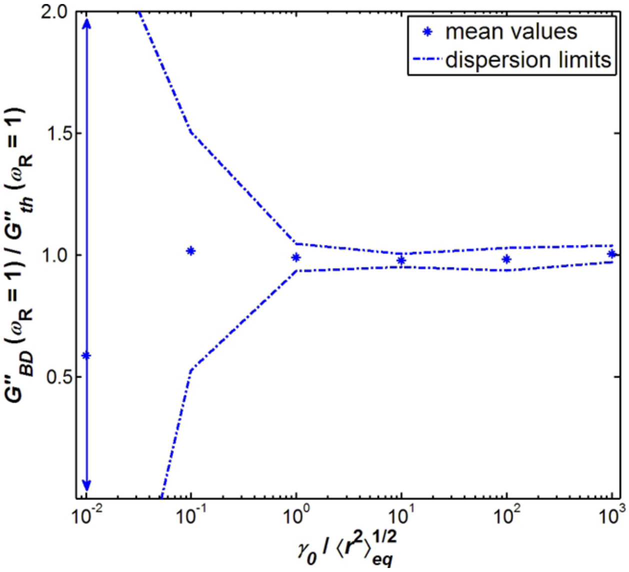

Fig. 8 BD prediction of the loss modulus at the characteristic frequency for a Hookean dumbbell model in function of the maximal shear strain applied. Maximal shear strain is normalized by the equilibrium end-to-end distance of a Hookean dumbbell model. H, ζ and ck_BT are fixed to 1 in a consistent system of units. A population of 10^3 dumbbells and a time step equal to $\lambda_H/100$ have been employed

a mean value equal to 0.99 ± 0.03 (95 % confidence) during 600 times steps. On the other hand, the out-of-diagonal components of the same tensor have an absolute mean value equal to 0.005 ± 0.063 (95 % confidence) during 600 iterations.

Dynamic Properties The linear viscoelastic behavior of a Hookean-dumbbell dilute solution can be obtained analytically. The constitutive equation of such system has a well-known solution, that results to be the same of a *convected* Jeffreys model, also known as the *Oldroyd-B model* [28]. Using such constitutive equation, the complex modulus of a Hookean-dumbbell dilute solution writes as follows:

$$G' = \frac{ck_BT\lambda_H^2\omega^2}{1+(\lambda_H\omega)^2} \tag{51}$$

$$G'' - \eta_s\omega = \frac{ck_BT\lambda_H\omega}{1+(\lambda_H\omega)^2} \tag{52}$$

The BD algorithm employed to estimate the dynamic response of a suspension submitted to a small-amplitude oscillatory strain was previously described in Sect. 2. An explicit integration scheme is implemented in the BD simulation and the Kramers expression is employed to compute the shear stress tensor. Using a time step equal to $\lambda_H/100$ and a population of 10^3 dumbbells (convergent simulation parameters at no-flow conditions), the BD performance is checked in Fig. 8 by plotting the loss modulus at the characteristic frequency ($\omega = \lambda_H^{-1}$) in function of the maximal imposed strain.

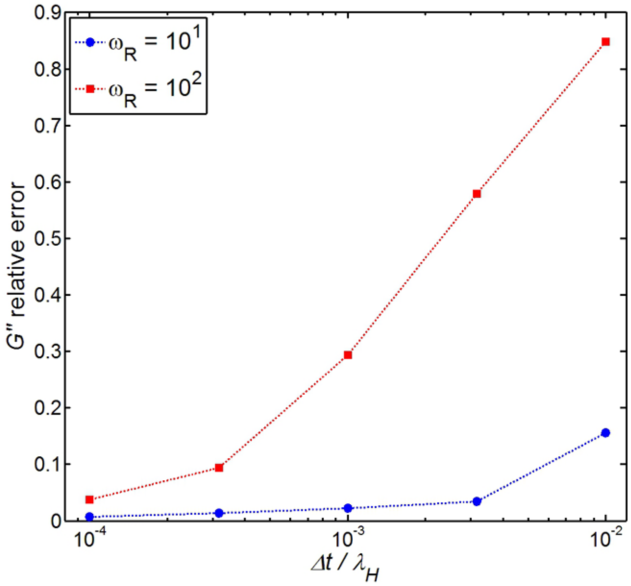

Fig. 9 Relative error of the BD prediction for the loss modulus at high frequencies in function of the time step. H, ζ and ck_BT are fixed to 1 in a consistent system of units. A population of 10^3 dumbbells has been employed. Relative error is defined as follows: $|(\log G''_{\mathrm{BD}}(\omega_R) - \log G''_{th}(\omega_R))/\log\Theta|$, where $\Theta = G'_{th}(\omega_R = 10^2)/G''_{th}(\omega_R = 10^2)$ is the maximal interval of complex modulus variation in the tested frequency interval

Bead-spring models are not able to describe the decrease of viscosity when shear rate is enhanced [28]. This fact is confirmed by Fig. 8 where the BD estimation of the loss modulus at the characteristic frequency appears independent of the maximal shear strain applied. However, a huge numerical dispersion is observed at low strains. This numerical noise is given by the stochastic nature of the Brownian forces when the magnitude of those ones is equal or higher than the magnitude of the flow-induced forces. In fact a narrower dispersion was obtained when implementing a more precise random number generation algorithm.

At low frequencies the convergence of the integration scheme is guaranteed by the criteria obtained for the no-flow conditions. That is truth because at low frequencies, system motion is controlled essentially by the thermal activity. At high frequencies, nevertheless, additional considerations are needed in order to satisfy the convergence of the integration scheme. In fact, at higher frequencies than the characteristic one, flow-induced forces become the controlling factor of the kinematics of the system and the relative importance of the stochastic forces is progressively reduced. For that reason at high frequencies, as the intensity of the flow field increases time step must to be gradually refined in order to guarantee convergence towards the central values. To show this fact, in Fig. 9 the BD convergence at two high frequencies ($\omega_R = 10$ and $\omega_R = 10^2$) is deployed by plotting the relative error of the loss modulus estimation for a population of 10^3 dumbbells with respect to the time step implemented.

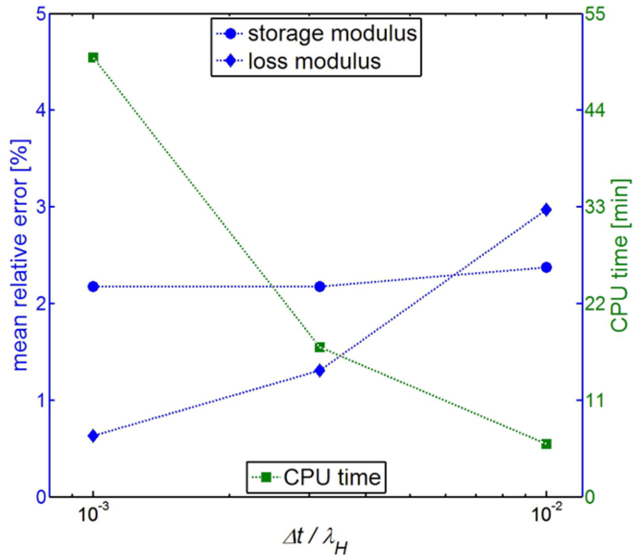

Fig. 10 Mean relative error of the BD prediction of the storage and loss modulus (for a Hookean dumbbell model) and total computational time in function of the time step implemented. Mean relative errors are calculated as the average of 34 points distributed homogeneously in a reduced frequency range going from 10^{-2} to 10^{2}. Relative error is defined as follows: $|(\log G'_{\mathrm{BD}}(\omega_R) - \log G'_{th}(\omega_R))/\log \Theta|$, where $\Theta = G'_{th}(\omega_R = 10^2)/G'_{th}(\omega_R = 10^{-2})$ is the maximal interval of complex modulus variation in the tested frequency interval. H, ζ and ck_BT are fixed to 1 in a consistent system of units. A population of 5000 dumbbells has been employed

From Fig. 9, at a reciprocal frequency equal to 10^1, a diminution of the relative error from 16 % to 0.7 % is appreciated when the time step is reduced from $\lambda_H/100$ to $\lambda_H/10^4$. An even more pronounced effect of the time step is observed for a reciprocal frequency of 10^2, given the high sensitivity of the sine function around zero (phase angle tends to zero as frequency increases). In that case, a diminution of the relative error from 84 % to 4 % is noticed for the same refining of the time step. On the other hand, storage modulus is much less sensitive to the time step than the loss modulus in the high frequency regime because of the less variability of the cosine function with respect to the sine function around zero. For example, at $\omega_R = 10^2$, a reduction of the relative error going from 1.6 % to less than 0.1 % is observed when the time step is diminished from $\lambda_H/100$ to $\lambda_H/10^4$.

In Fig. 10 the global BD performance to predict the complex modulus in a frequency sweep test within a representative frequency interval is presented.

BD performance is depicted by plotting the mean relative error for the storage and loss modulus for 34 frequencies homogeneously distributed within an interval of reduced frequencies going from 10^{-2} to 10^2 in function of the time step. A population of 5000 dumbbells is used in the BD simulations. In all the sweep frequency tests a practically constant mean relative error for the storage modulus is obtained (∼2 %). This inaccuracy in the prediction of the storage modulus is coming mainly from the low frequencies regime ($10^{-2} \le \omega_R \le 10^{-1}$) given the high variability of the cosine function approaching $\pi/2$ (phase angle tends to this value as frequency diminishes). No improvement in convergence to the central values is appreciated when refining the time step because the origin of the dispersion is not associated with the integration scheme, but with the natural fluctuations of the stochastic forces that control the kinematics of the dumbbell at low velocities. Implementation of a more sophisticated algorithm for generating random numbers is required to improve the convergence of the storage modulus at low frequencies. In fact, the list of pseudo-random numbers generators is continuously growing as reflect of the remaining challenges in this computational art [3, 70]. On the contrary, a considerable improvement in the loss modulus prediction is checked as smaller time steps are employed. A reduction of the mean relative error from 3.0 % to 0.6 % is obtained when time step is shortened from $\lambda_H/100$ to $\lambda_H/10^3$. This improvement in convergence for the loss modulus is related directly to the better accuracy at high frequencies, as showed before in Fig. 9. As expected, a linear increment on the computational time (4× Intel Itanium® 2 Monticito 1400 MHz) is observed as the time step is shortened.

3.4.2 *The Multi-Bead-Spring Chain*

The analytical expression of the constitutive equation for the Rouse model (composed of $n-1$ Hookean springs) is well-known. It results to be the linear superposition of $n-1$ Hookean dumbbells with a spectrum of relaxation times λ_j following the next normal modes [28]:

$$\lambda_j = \frac{\zeta/2H}{4\sin^2(j\pi/2n)} \tag{53}$$

When a dilute solution of Rouse chains is submitted to a small-amplitude oscillatory deformation test, the complex modulus contribution given by the chains writes as follows:

$$G' = ck_BT \sum_{j=1}^{n-1} \frac{\lambda_j^2\omega^2}{1+(\lambda_j\omega)^2} \tag{54}$$

$$G'' - \eta_s\omega = ck_BT \sum_{j=1}^{n-1} \frac{\lambda_j\omega}{1+(\lambda_j\omega)^2} \tag{55}$$

In principle, the numerical considerations extracted from the BD simulations with Hookean-dumbbells can be extrapolated to the BD simulations of multi-bead-spring chains. In Figs. 11 and 12 the BD predictions for the complex modulus of Rouse chains with 1, 10 and 50 springs are compared. All BD simulations are carried out using a population of 5000 chains, a number proved to provide a good compromise between prediction accuracy and computational time (see Fig. 6). A frequency sweep test is carried out on 34

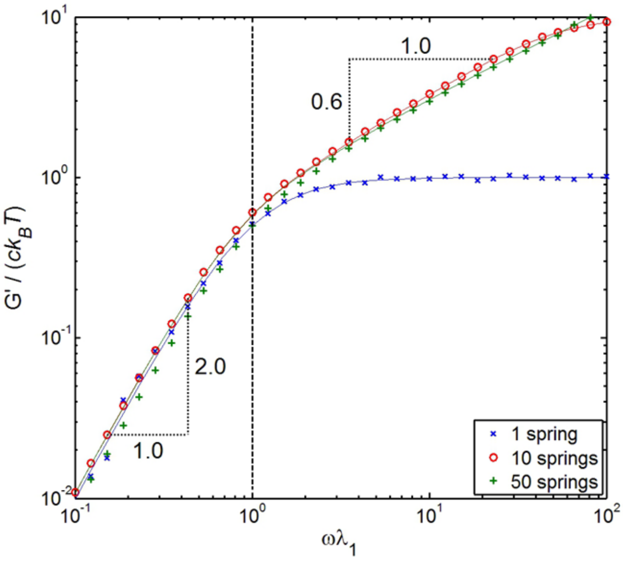

Fig. 11 BD prediction of the storage modulus in function of the reduced frequency for three Rouse chains: 1-*spring*, 10-*springs* and 50-*springs*. Analytical curves are represented by solid lines. H, ζ and ck_BT are fixed to 1 in a consistent system of units. A population of 5000 chains has been employed

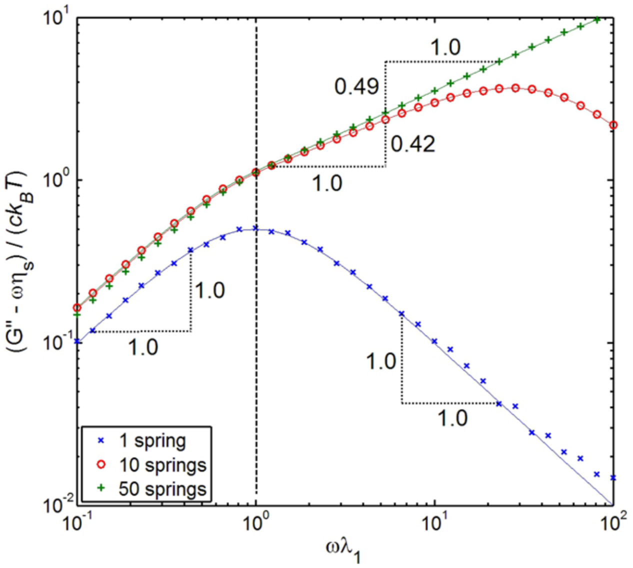

Fig. 12 BD prediction of the loss modulus in function of the reduced frequency for three Rouse chains: 1-*spring*, 10-*springs* and 50-*springs*. Analytical curves are represented in solid lines. H, ζ and ck_BT are fixed to 1 in a consistent system of units. A population of 5000 chains has been employed

points homogeneously distributed in a reciprocal frequency interval going from 10^{-1} to 10^2. A constant time step equal to $\lambda_{n-1}/500$ was implemented, where λ_{n-1} is the shortest time of the relaxation times spectra. This length of the time step was demonstrated to provide also a good compromise between accuracy and computational cost (see Fig. 10).

From Fig. 11 is observed that the prediction of the storage modulus is less accurate at low frequencies. It was already mentioned that the inaccuracy at low frequencies comes from the random number generation; hence improvement in the accuracy of the BD prediction is subjected to the implementation of more sophisticated algorithms of random number generation. Quality of the random number generation is only reflected at low frequencies because, at this regime of flow, the dynamics of the multi-bead-spring chain is governed by the randomizing thermal forces; whereas at high frequencies the statistical errors of the computational random number generation are masked by the effects of the external-imposed flow-field.

Mean relative errors for the BD prediction of the storage modulus are 0.9 %, 0.2 % and 0.1 % for the single Hookean dumbbell, the 10-springs and the 50-springs chain respectively. BD simulations are capable to predict the apparition of new relaxation processes when increasing the number of springs. Notice the elastic enhancement at high frequencies, going from the characteristic plateau of the Hookean dumbbell model to non-zero slopes of the storage modulus in function of the frequency; for instance 0.6 for the 10-springs and 50-springs chain around a reduced frequency of 10. It is worth to mention that Rouse theory predicts a storage modulus evolving with $\omega^{0.5}$ for very long chains ($n > 300$). Tendency towards this limiting value has been registered by the BD simulations; a slight reduction of the storage modulus slope in the high frequency range is appreciated when going from 0.65 for the 10-springs chain to 0.61 for the 50-springs one.

In Fig. 12 the BD predictions of the loss modulus in function of the frequency are plotted for the same Rouse chains presented in Fig. 11. For the Hookean dumbbell system, inaccuracy in the BD prediction is concentrated at high frequencies, on the contrary of the storage modulus. In this case, given the low values of loss modulus at high frequencies, error is coming from a bad resolution of the integration scheme when the phase angle approaches 0. Shorter time steps are required in this frequency window (10^1 to 10^2), but it is important to say that the model response at those frequencies lacks of physical meaning too.

BD simulations are able to correctly predict the evolution of the loss modulus in the high frequency range. Observe, for instance, the linear decrease of the loss modulus for the dumbbell system and the linear increases of the loss modulus for the 10-springs and 50-springs chains at high frequencies. In the high frequency range, the predicted slopes of 0.42 and 0.49 for the 10-springs and 50-springs chains respectively, are also consistent with the maximal limiting value of 0.5 given by the Rouse theory. BD simulations show that when increasing the number of springs, storage and loss moduli tend converging towards the same values in the high frequency range, as predicted by Rouse theory for large number of springs ($n > 300$).

Mean relative errors for the loss modulus prediction are 1.6 %, 0.3 % and 0.7 % for the Hookean dumbbell, the 10-springs and the 50-springs chain respectively. CPU[1] time (4× Intel Itanium® 2 Monticito 1400 MHz) goes up from 15 minutes to 10 hours when passing from 1-spring to 10-springs, an impressive increment of the computational cost. This fact is explained by the longer main relaxation times when dealing with bigger number of springs that are traduced in longer stabilization steps in the BD algorithm given in Sect. 2, specially in the high frequency range. Additionally, the short time steps required in an explicit integration scheme imply longer analytical steps in the implemented BD algorithm, specially in the low frequency range.

3.5 The Zimm Model

Unlike the Rouse model, in Zimm theory hydrodynamic interaction is taken into account. From a formal point of view, the kinematic description is exactly the same as that one of the Rouse model, except for the hydrodynamic drag force, where an additional term is considered to account for the local variation in the bulk flow field caused by the motion of the other beads in the multi-bead-spring chain. Pioneer works on hydrodynamic interaction inside flexible macromolecules are attributed to Kirkwood and Riseman [30, 71]. Zimm adapted the Kirkwood's results in hydrodynamic interaction to the multi-bead-spring model in order to estimate the viscoelastic, birefringence and dielectric properties of dilute polymer solutions. Zimm found the analytical solution of the model by using a transformation to normal coordinates [58].

The particularities of the implementation of a BD simulation for a multi-bead-spring model with hydrodynamic interaction can be revealed by transforming the general expression for the bead velocity given in Eq. (28). Neglecting external forces and supposing an isotropic friction tensor, the generalized stochastic differential equation in Eq. (28) can be rewritten as follows:

$$\frac{d\mathbf{r}_i}{dt} = -\sum_j \boldsymbol{\Omega}_{ij} \cdot \mathbf{F}_j^{(h)} + \left[\boldsymbol{\kappa}(\mathbf{r}_i) \cdot \mathbf{r}_i\right] + \frac{\mathbf{F}_i^{(\phi)}}{\zeta} + \frac{\mathbf{F}_i^{(b)}}{\zeta} \tag{56}$$

where the local hydrodynamic interaction term $\mathbf{v}_i'$ has been approximated by using the Oseen-Burgers hydrodynamic tensor. As the balance of forces over each bead is zero (inertialess Langevin equation) the hydrodynamic force in Eq. (56) can be written in terms of the other forces:

$$\frac{d\mathbf{r}_i}{dt} = \sum_j \boldsymbol{\Omega}_{ij} \cdot \left[\mathbf{F}_j^{(\phi)} + \mathbf{F}_i^{(b)}\right] + \left[\boldsymbol{\kappa}(\mathbf{r}_i) \cdot \mathbf{r}_i\right] + \frac{\mathbf{F}_i^{(\phi)}}{\zeta} + \frac{\mathbf{F}_i^{(b)}}{\zeta} \tag{57}$$

Reordering and bringing together common terms:

$$\frac{d\mathbf{r}_i}{dt} = \left[\boldsymbol{\kappa}(\mathbf{r}_i) \cdot \mathbf{r}_i\right] + \frac{1}{\zeta}\sum_j \mathbf{HI}_{ij} \cdot \mathbf{F}_j^{(\phi)} + \frac{1}{\zeta}\sum_j \mathbf{HI}_{ij} \cdot \mathbf{F}_j^{(b)} \tag{58}$$

where $\mathbf{HI}_{ij} = \delta_{ij}\,\boldsymbol{\delta} + \zeta\,\boldsymbol{\Omega}_{ij}$ is called the Hydrodynamic Interaction (HI) matrix associated with a given pair of beads i and j inside the chain. Finally, through the fluctuation-dissipation theorem the stochastic differential Eq. (58) for the bead velocity in a multi-bead-spring chain with hydrodynamic interaction takes the form [1]:

$$\frac{d\mathbf{r}_i}{dt} = \left[\boldsymbol{\kappa}(\mathbf{r}_i) \cdot \mathbf{r}_i\right] + \frac{1}{\zeta}\sum_j \mathbf{HI}_{ij} \cdot \mathbf{F}_j^{(\phi)} + \sqrt{\frac{2k_BT}{\zeta}}\sum_j \mathbf{C}_{ij} \cdot \frac{d\mathbf{W}_j}{dt} \tag{59}$$

where $\mathbf{HI}_{ij} = \mathbf{C}_{ij} \cdot \mathbf{C}_{ij}^T$. Hydrodynamic interaction in multi-bead-spring chains is tackled rigorously with Eq. (59), but at present it cannot be solved in closed form [1]. To circumvent this difficulty, Zimm theory replaces the variable Oseen-Burgers tensors by their equilibrium averages. By using the equilibrium-averaged distance between two beads inside a Rouse chain $\langle r_{ij}\rangle_{eq}$ (see [28]) the equilibrium-averaged Oseen-Burgers hydrodynamic tensor given in Sect. 3.1 can also be expressed as follows [58]:

$$\langle \boldsymbol{\Omega}_{ij}\rangle_{eq} = \frac{1-\delta_{ij}}{6\pi\eta_s}\sqrt{\frac{2H}{\pi k_BT|i-j|}}\,\boldsymbol{\delta} \quad \text{for } i \neq j \tag{60}$$

When introducing Eq. (60) into Eq. (59) it is found that $\mathbf{HI}_{ij} = \mathbf{HI}$ and $\mathbf{C}_{ij} = \mathbf{C}$ where $\mathbf{HI} = \mathbf{C} \cdot \mathbf{C}^T$. As noticed, in Zimm theory HI tensor becomes a $n \times n$ constant matrix whose components $(\mathbf{HI})^{ij}$ are given by the next formula:

$$(\mathbf{HI})^{ij} = \delta_{ij} + (1-\delta_{ij})h^*\sqrt{\frac{2}{|i-j|}} \tag{61}$$

where h^* is the hydrodynamic interaction parameter according to Thurston and Peterlin [72]:

$$h^* = \frac{\zeta}{\eta_s}\sqrt{\frac{H}{36\pi^3 k_BT}} \tag{62}$$

---

[1] Central Processing Unit.

where ζ is the bead friction coefficient, η_s is the solvent viscosity and H is the Hookean-spring constant. The hydrodynamic interaction parameter h^* can be expressed also as the ratio of the bead radius to the root-mean-square distance between two beads linked by a spring at equilibrium. In that context, it is expected that h^* is lower than 0.5 [1]. From a practical point of view, experimental viscoelastic data for several polymer solutions are generally well represented by Zimm chains of several hundreds of beads with hydrodynamic interaction parameters between 0.1 and 0.2 [73].

From a numerical point of view (BD approach) integration of the stochastic differential equation for a Zimm chain (Eq. (59)) does not represent an additional cost with respect to the Rouse chains (Zimm hydrodynamic interaction matrix is constant). In addition, equations employed to describe the kinematics and to compute the shear-stress tensor are quite similar for both models. Hence, the numerical considerations about the number of trajectories required and the time step (in an explicit integration scheme) inferred for Rouse chains can, in principle, be extended to the BD simulations of Zimm chains.

It seems that the calculation of the matrix $\mathbf{C}_{ij}$ has a numerical relevance when general hydrodynamic interaction (i.e. based on the general expression of the Oseen-Burgers tensor) for chains with large number of beads ($n > 300$) is considered, owing to the fact that the hydrodynamic interaction matrix is recalculated at each time step. Classical Cholesky decomposition is expensive, scaling with the cube of the number of beads [1]. In response, Fixman proposed two alternative numerical methods to calculate the square-root of the hydrodynamic interaction matrix: one by Newton iteration and the other one by Chebyshev polynomial decomposition [74]. Implementation of the last polynomial approximation for the square-root of the hydrodynamic interaction matrix in a BD framework is detailed elsewhere [1]; this method roughly scales with $n^{9/4}$ per time step. In any case, previous numerical issue has a reduced impact on the BD simulation of Zimm chains due to the fact that the equilibrium-averaged hydrodynamic interaction matrix is constant and the required decomposition is carried out just one time for all the simulation.

Given the fact that hydrodynamic interaction is approximated by the equilibrium averaged Oseen-Burgers tensor, a close-form of the constitutive equation can be derived for the Zimm model in total analogy with that one of the Rouse model [3, 28]. For that reason, expressions for the contribution of Zimm chains to the complex modulus of their dilute suspensions have the same form that the equations for Rouse chains (Eqs. (54) and (55)):

$$G' = ck_BT \sum_{j=1}^{n-1} \frac{\tilde{\lambda}_j^2\omega^2}{1+(\tilde{\lambda}_j\omega)^2} \tag{63}$$

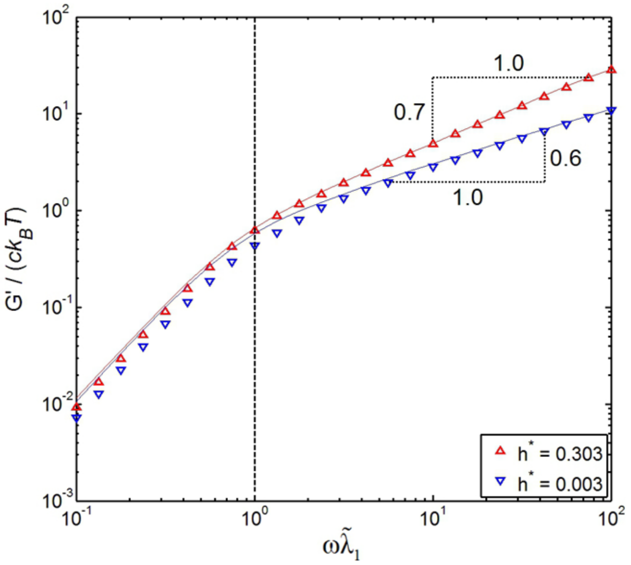

Fig. 13 BD prediction of the storage modulus in function of the reduced frequency for two 50-springs Zimm chains with high hydrodynamic interaction ($h^* = 0.303$) and very low hydrodynamic interaction ($h^* = 0.003$). Analytical curves are represented in *solid lines*. H, ζ and ck_BT are fixed to 1 in a consistent system of units. A population of 10^4 dumbbells has been employed

$$G'' - \eta_s\omega = ck_BT \sum_{j=1}^{n-1} \frac{\tilde{\lambda}_j\omega}{1+(\tilde{\lambda}_j\omega)^2} \tag{64}$$

The only difference lies on the relaxation time spectra. In the Zimm model the time constants are dictated by:

$$\tilde{\lambda}_j = \frac{\zeta}{2H\tilde{a}_j} \tag{65}$$

where $\tilde{a}_j$ are the eigenvalues of the modified Rouse matrix $\tilde{\mathbf{A}}$ whose components $(\tilde{\mathbf{A}})^{ij}$ are given by:

$$(\tilde{\mathbf{A}})^{ij} = \sum_v \sum_u \bar{B}_{iv}(\mathbf{HI})^{vu}\bar{B}_{ju} \tag{66}$$

and $\bar{B}_{vu}$ is a scalar operator following the next formula [28]:

$$\bar{B}_{vu} = \delta_{v+1\,u} - \delta_{v\,u} \tag{67}$$

This analytical solution allows us to evaluate easily the performance of the BD simulation predicting the linear viscoelastic behavior of multi bead-spring systems with equilibrium-averaged hydrodynamic interaction. Figures 13 and 14 compare the BD predictions of the complex modulus for a 50-springs Zimm chain with two different hydrodynamic interaction parameters. A frequency sweep test is carried out over 25 points homogeneously distributed in a reduced frequency interval going from 10^{-1} to 10^2.

From Fig. 13 is observed that the BD prediction of the storage modulus is more accurate for the high hydrodynamic interaction case than the low one. In fact, the mean relative

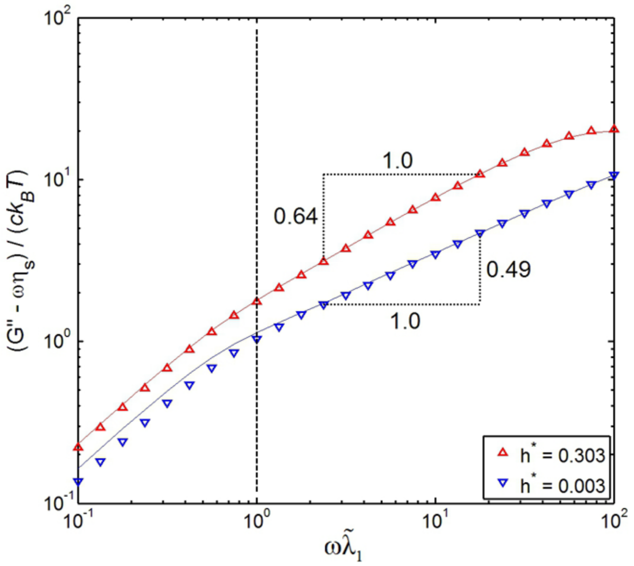

Fig. 14 BD prediction of the loss modulus in function of the reduced frequency for two 50-springs Zimm chains with high hydrodynamic interaction ($h^* = 0.303$) and very low hydrodynamic interaction ($h^* = 0.003$). Analytical curves are represented in *solid lines*. H, ζ and ck_BT are fixed to 1 in a consistent system of units. A population of 10^4 dumbbells has been employed

error for the low value of h^* is about 2.7 % in comparison with the mean relative error of 0.8 % for the case of high h^*. The main source of inaccuracy is coming from the low frequency range. This is explained, as in the BD simulations with Rouse chains, by the statistical deviations originated in the numerical computation of the stochastic forces coupled with the relative dominance of the thermal forces as driving mechanism of the chain kinematics in the low frequency range. As a consequence, improvement of the accuracy at low frequencies depends on the implementation of more sophisticated random numbers generators.

On the other hand, BD simulations correctly predict the evolution of the storage modulus at high frequencies. Figure 13 shows the increase of the slope of G' going from 0.6 for the low hydrodynamic interaction case ($h^* = 0.003$) to 0.7 for the high hydrodynamic interaction case ($h^* = 0.303$), within the reduced frequency interval between 10^1 and 10^2.

In Fig. 14 the BD prediction of the loss modulus versus the frequency is plotted for the same Zimm chains presented in Fig. 13. Again better accuracy is obtained for the chain with higher hydrodynamic interaction. In fact, mean relative error goes down from 1.6 % to near 0.3 % when h^* is increased from 0.003 to 0.303. As observed for the storage modulus prediction, main source of error is coming from the low frequency regime.

BD performance at high frequencies is quite better. Simulations are able to correctly predict the change in the loss modulus slope when varying the relative importance of the hydrodynamic interaction. At low hydrodynamic interaction a Rouse-type slope is observed, whereas at high hydrodynamic interaction ($h^* = 0.303$), the slope of the loss modulus reaches a maximal value of 0.64 around a reduced frequency of 10. This prediction is consistent with the Zimm theory for very long chains (i.e. $n > 300$) and high hydrodynamic interaction (for instance, $h^* = 0.3$), where storage and loss moduli evolve linearly with $\omega^{2/3}$ [75]. On the other hand, in our BD simulation of 50-springs chains with high hydrodynamic interaction ($h^* = 0.303$) we have found $(G'' - \eta_s\omega)/G' = 1.67$ around a reduced frequency of 10, a result also in coherence with Zimm theory where a constant ratio $(G'' - \eta_s\omega)/G' = \sqrt{3}$ is predicted in the high frequency range.

4 BD of Generalized Bead-Rod Models

The fundamental difference between the bead-rod model and the bead-spring model lies in that the former has a finite contour length. This simple, but important fact is traduced directly in different rheological responses. On the other hand, a physical model with a finite contour length imposes subtle, but important numerical issues that are reflected in the BD implementation.

As mentioned in Sect. 1.2.1, historically bead-rod models were first proposed to emulate the structure of linear polymers in a coarse-grained fashion. Bead-rod model with fixed adjacent angles (as proposed by Flory [29]) constitute the first stage of coarse-graining in kinetic theory. In that model, rods are supposed to represent the bond length between two consecutive atoms in the backbone of the polymer chain. Simpler representations with fewer degrees of freedom have been extensively proposed. For instance, some polymer chains are quite bendable along certain number of monomer units, in those cases from 3 to 5 monomer units can be replaced by one non-bendable rod. Polymer flexibility is then mimicked by introducing some kind of bending potential between consecutive rods. Continuous version of this model is known as the worm-like chain, in which the thermal equilibrium configuration is a perfect straight filament. An even coarser model replaces from 10 to 20 monomer units by one rigid-rod; any notion of flexion hindering at this rod-scale is lost and the polymer chain is represented then by a freely-jointed multi-rod chain [28]. An ultimate scale in the coarse-graining process replaces a hundred of backbone atoms (or a ten of rods from the freely-jointed multi-rod model) by an *entropic* spring, so mechanical behavior of the macromolecule is represented by a multi-bead-spring chain model (showed in the previous Sect. 3). Despite that the historical motivation for the bead-rod model is linked to the polymer science, this representation has been extensible applied to emulate the mechanical behavior of other structures as short DNA, rod-like virus, collagen fibrils, synthetic polymers and CNTs.

Bead-rod models have escaped from a deeply development in the kinetic theory framework with respect to the bead-spring counterparts because the inextensibility condition imposes the use of generalized coordinates [76]. This mathematical complexity explains why only some results in zero-shear, steady and linear unsteady flows have been obtained for this model [77, 78].

In the case of bead-rod models, BD simulations appear as an interesting alternative approach to by-pass the complex mathematical-treatment of the diffusion equation. Anyway, the use of constraints also implies to be careful during a BD implementation, particularly in terms of the integration scheme and the stochastic forces generation.

Bead-rod models have been particularly studied for approaching the mechanical behavior of bead-spring chains with very stiff Fraenkel-typesprings (non-zero natural length). Intuitively a very stiff Fraenkel spring could be replaced by a rigid rod for the sake of mathematical simplicity. However, it is found that this limit is a very singular one. In fact, bead-rod chains and bead-spring chains differ even in the limit of infinitely stiff springs. For instance, the configurational distribution of a freely-jointed multi-bead-rod chain at thermal equilibrium is found to be different from a random-walk distribution, which is typical for a freely-jointed multi-bead-spring chain [28]. This difference has been confirmed by molecular and Brownian dynamics simulations [5, 79–81] and statistical mechanics calculations [82, 83]. On the other hand, it has been showed that introducing a corrective potential force (function of the chain configuration) into the multi-bead-rod chain formulation is possible to mimic the behavior of multi-bead-spring chains [82, 84]. This result strongly promoted the use of BD simulations for studying the dynamical behavior of polymers by using the multi-bead-rod model and the corrective potential approach [66, 74, 85–89]. In this work, the intrinsic behavior of multi-bead-rod models is tackled; the bead-spring chain statistics is not intended to be mimicked.

In what follows, the basis of a BD implementation for a generalized multi-bead-rod chain with an isotropic friction tensor and in absence of hydrodynamic interaction is presented. We focus in two classical cases: the freely-jointed chain or Kramers model and the non freely jointed chain that corresponds to a discrete version of the worm-like chain model.

4.1 Kinematic and Dynamic Formulation

Constraints can be treated mathematically in a generalized coordinate system (based on the configuration of the chain) or in a Cartesian coordinate system, case in which constraint forces are required to complement the kinematic description. Going and coming back between those two frameworks requires a lot of care in order to conserve a proper equivalence at the levels of the FP equation and the differential stochastic equation [3].

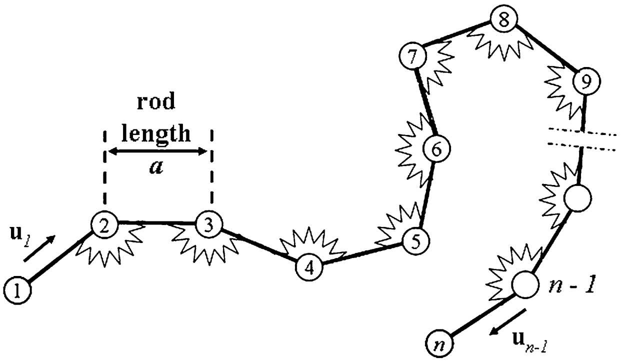

Fig. 15 Non-freely jointed multi-bead-rod model composed of n beads and $n-1$ rods of length a. Bending potential between rods in the multi-bead-rod chain model is mimicked with a hypothetical flexion spring

From a formal point of view a general, expression of the FP equation for a multi-bead-rod model with no internal potentials, including hydrodynamic interaction and anisotropic friction tensor, was given by Curtiss using generalized coordinates [28]. This diffusion equation is coherent with the equilibrium statistical mechanics for a real bead-rod chain with equal bead masses. A detailed description of the development of an equivalent stochastic differential equation in the strong sense was given by Öttinger [3]. He also showed a particular transformation of that differential stochastic equation from generalized to Cartesian coordinates. In doing so, not only an explicit definition of the rod inextensibility is required, but also a metric potential force, depending on the chain configuration, has to be considered in order to respect the equivalence (at least in a weak sense) with the FP equation developed by Curtiss. Interestingly, it is found that the negative of such metric force is equal to the corrective potential force added in the BD numerical algorithms of multi-bead-rod chains intended to mimic the behavior of multi-bead-spring chains.

For the sake of simplicity, BD implementation in a Cartesian coordinate system is employed in this paper. Metric potential forces are neglected without incurring in error because, in one hand, the drag acting on the simulated multi-bead-rod chain is supposed characterized by an isotropic friction tensor and, on the other hand, no hydrodynamic interactions are considered.

Let us consider the multi-bead-rod chain model showed in Fig. 15. Multi-bead-rod chain is constituted of n beads joined by $n-1$ non-bendable rigid rods of length a.

Position of the bead-rod chain can be instantaneously defined in a Cartesian reference system by the ensemble of bead positions $\mathbf{r}_i$ and the center of mass of the chain $\mathbf{r}_c$ (see

Eq. (14)). Orientation of each rod is given by the vector $\mathbf{u}_j$, which is a unit vector collinear to the rod connecting beads j and $j+1$. $\mathbf{u}_j$ is defined as follows:

$$\mathbf{u}_j = (\mathbf{r}_{j+1} - \mathbf{r}_j)/a \tag{68}$$

Rods are supposed infinitely rigid. Physical length of the system is equivalent to the total length of the multi-bead-rod chain $(n-1)a$. Existence of an internal bending potential, coming from a hypothetical flexion spring between each pair of rods, is considered with the purpose of mimic the bending flexibility of the filament-like system. Introduction of a non-zero bending potential complicates the FP formulation and make of the BD simulation a privileged numerical approach. On the other hand, multi-bead-rod chains are supposed suspended into a Newtonian solvent (viscosity η_s) at temperature T. Concentration of the bead-rod chains is defined in terms of c chains per volume unit. High dilution hypothesis is made, so no inter-chain interaction is considered. Moreover, flow field acting on the suspension is assumed to be homogeneous. Beads are considered the centers of hydrodynamic resistance; so all forces are concentrated on beads. In what follows, forces acting on the multi-bead-rod chains are described in more detail.

- Hydrodynamic drag force acting on bead i, $\mathbf{F}_i^{(h)}$

  Physical origin and mathematical description of this force are the same given for the multi-bead-spring model (see Sect. 3.1). As mentioned before, hydrodynamic interaction is neglected and an isotropic friction coefficient is supposed in order to avoid the calculation of metric potential forces.
- Constraint forces acting on bead i, $\mathbf{F}_i^{(\lambda)}$

  This force takes into account the sum of rod tensions acting on each bead i. Rod tension λ_j corresponds to the module of the instantaneous force emerging on bead j for maintaining the distance between beads j and $j+1$ at a constant value a. This force is transmitted along the rigid-rod and is manifested on bead $j+1$ with an opposite sign. Mathematically, total constraint force on bead i can be expressed as follows:

$$\mathbf{F}_i^{(\lambda)} = -\sum_{j=1}^{n-1} \mathbf{n}_{ij}\lambda_j \tag{69}$$

  where $\mathbf{n}_{ij}$ is a linear operator defined as follows:

$$\mathbf{n}_{ij} = \mathbf{u}_j(\delta_{i\,j+1} - \delta_{i\,j}) \tag{70}$$

- Internal bending potential force acting on bead i, $\mathbf{F}_i^{(\phi)}$

  Based on the viscoelastic theory of concentrated solutions of semi-flexible polymers [90], Pasquali and Morse defined a discrete bending potential for a multi-bead-rod model based on the worm-like chain continuous model [87]:

$$\phi = -\frac{K_b}{a}\sum_{i=2}^{n-1} \mathbf{u}_i \cdot \mathbf{u}_{i-1} \tag{71}$$

  where ϕ is the internal-bending potential and K_b is a bending rigidity constant. The bending potential defined in Eq. (71) can be understood as coming from the mechanical action of a torsion spring between two consecutive rods. In this case, local bending energy is proportional to the cosine of the internal angle between two consecutive rods. In other words, minimal internal bending energy state is achieved when all rods are completely aligned. Usually, this linear relationship is restricted to small flexion angles. Obviously, definitions of non-linear bending potentials are required for large deformation scenarios. Bending force acting on bead k can be obtained as the derivate of the bending potential in Eq. (71) with respect to the position of bead k:

$$\mathbf{F}_k^{(\phi)} = -\frac{\partial\phi}{\partial\mathbf{r}_k} = \frac{K_b}{a}\sum_{i=2}^{n-1}\frac{\partial(\mathbf{u}_i\cdot\mathbf{u}_{i-1})}{\partial\mathbf{r}_k} \tag{72}$$

  To simplify the derivate on the right side of Eq. (72), next identity is employed [87]:

$$\frac{\partial}{\partial\mathbf{r}_k}\mathbf{u}_i = \frac{1}{a}(\delta_{k\,i+1} - \delta_{k\,i})(\boldsymbol{\delta} - \mathbf{u}_i \otimes \mathbf{u}_i) \tag{73}$$

- Brownian force acting on bead i, $\mathbf{F}_i^{(b)}$

  As in all coarse-grained models, Brownian forces approach the change of momentum of a bead i coming from the thermal activity of the solvent molecules surrounding bead i. Accounting for faster processes than the coarse-grained model motion, Brownian forces are computed as an stochastic process. In a model without constraints (free particles, bead-spring chains), Brownian forces follow a normal distribution with first and second moments defined previously by Eqs. (25) and (26), respectively. However, as the generalized friction of the bead-rod system is modified by the presence of constraints, random forces must reflect the inextensibility of rods [86].

  An algorithm proposed to tackle properly last issue requires that Brownian forces are geometrically projected random forces. Geometrical projection of random forces on bead-rod chains is absolutely necessary when the bead-spring statistics want to be mimicked (using of corrective potential forces and a mid-step integration algorithm) or an anisotropic friction tensor is considered [89].

  On the other hand, when dealing with free-draining bead-rod chains in which each bead is characterized by an isotropic friction coefficient ζ, geometrical projection of Brownian forces is redundant [89] and same kinematics is obtained by using unprojected Brownian forces. To show last fact (and present in parallel the structure of the geometrical projection algorithm), let us take the example of one single rigid rod embedded into a solvent bath at temperature T, no external flow is imposed. Supposing an isotropic friction coefficient, the force balances on the two mass-less beads write:

$$-\zeta\dot{\mathbf{r}}_1 - \mathbf{n}_{11}\lambda_1 + \mathbf{F}_1^{(b)} = m_1\ddot{\mathbf{r}}_1 = \mathbf{0} \tag{74}$$

$$-\zeta\dot{\mathbf{r}}_2 - \mathbf{n}_{21}\lambda_1 + \mathbf{F}_2^{(b)} = m_2\ddot{\mathbf{r}}_2 = \mathbf{0} \tag{75}$$

In order to satisfy the inextensibility of the rigid-rod, next condition has to be imposed over the bead velocities:

$$0 = \sum_{i=1}^{2} \dot{\mathbf{r}}_i \cdot \mathbf{n}_{i1} = (\dot{\mathbf{r}}_2 - \dot{\mathbf{r}}_1)\cdot\mathbf{u}_1 \tag{76}$$

Placing the bead velocities from Eqs. (74) and (75) into Eq. (76) we obtain:

$$\frac{1}{\zeta}\left(-\lambda_1\mathbf{u}_1 + \mathbf{F}_2^{(b)} - \lambda_1\mathbf{u}_1 - \mathbf{F}_1^{(b)}\right)\cdot\mathbf{u}_1 = 0 \tag{77}$$

Equation (77) can be rewritten also as follows:

$$2\lambda_1 = \sum_{i=1}^{2} \mathbf{F}_i^{(b)} \cdot \mathbf{n}_{i1} = \left(\mathbf{F}_2^{(b)} - \mathbf{F}_1^{(b)}\right)\cdot\mathbf{u}_1 \tag{78}$$

Previous equation resumes the conditions imposed over the Brownian forces in order to satisfy the inextensibility condition. Two numerical algorithms for the random forces generation can be considered at this point. The first takes into account the contribution of random forces to the rod tensions and implies to calculate λ_1 at each time step from Eq. (78). In this case, random forces are generated like in the BD simulations of bead-spring models and the predictor-corrector integration scheme (Sect. 4.2.2) is required. In the second, contributions of random forces to the rod tension are neglected ($\lambda_1 = 0$) and unconstrained random forces have to be projected in order to satisfy $0 = \sum_{i=1}^{2} \mathbf{F}_i^{(b)} \cdot \mathbf{n}_{i1}$. This last expression determines the starting point of the geometrical projection algorithm. In order to obtain projected random forces $\mathbf{F}_i^{(b)'}$, it is necessary to substrate the "hard" component of the unconstrained Brownian forces $\hat{\eta}_1$ along the rod direction as follows:

$$\mathbf{F}_i^{(b)'} = \mathbf{F}_i^{(b)} - \mathbf{n}_{i1}\hat{\eta}_1 \tag{79}$$

The "hard" component of the unconstrained Brownian forces can be obtained from the solution of the next equation [89]:

$$\hat{G}\hat{\eta}_1 = \sum_{i=1}^{2} \mathbf{F}_i^{(b)} \cdot \mathbf{n}_{i1} \tag{80}$$

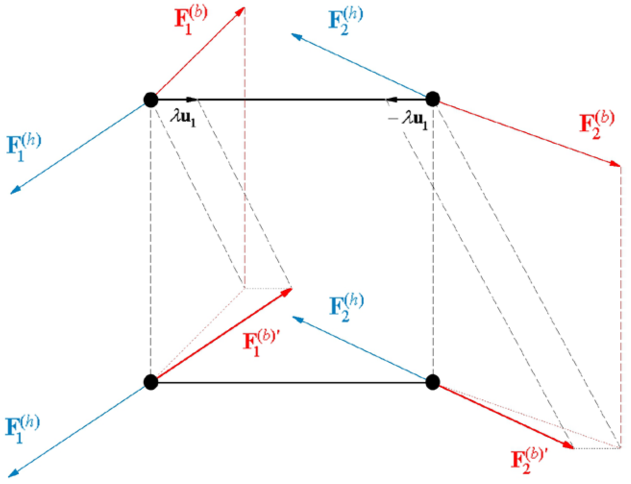

Fig. 16 Example of the geometrical projection of Brownian forces in a quiescent bi-dimensional single rigid-rod (no external-flow). An isotropic friction coefficient is supposed. In the *upper rod* no geometrical projection has been carried out, hence tension force is considered. In the *lower rod*, geometrical projection of Brownian forces absorbs the rod tension; observe that hydrodynamic forces are not modified

where $\hat{G} = \sum_i \mathbf{n}_{i1}\cdot\mathbf{n}_{i1} = 2$. From Eqs. (78) and (80) is easily inferred that $\hat{\eta}_1 = \lambda_1$. Hence, projected Brownian forces are $\mathbf{F}_1^{(b)'} = \mathbf{F}_1^{(b)} + \lambda_1\mathbf{u}_1$ and $\mathbf{F}_2^{(b)'} = \mathbf{F}_2^{(b)} - \lambda_1\mathbf{u}_1$. A graphic example of this projection in a bi-dimensional framework is showed in Fig. 16. Extension of previous algorithm for a multi-bead-rod case is straightforward and has been detailed elsewhere [85, 86].

Nevertheless, as mentioned before, geometrical projection of Brownian forces for a constrained system with an isotropic friction tensor is redundant because, as observed for the one-rod example in Fig. 16, projection of random forces has no consequences on the rod kinematics as hydrodynamic forces and rod velocity are not altered. In other words, considering a constant friction coefficient, rod kinematics depends exclusively on the orthogonal component of the Brownian forces with respect to the rod vector and this component is not modified by the geometrical projection algorithm.

- External forces acting on bead i, $\mathbf{F}_i^{(e)}$

  As mentioned before, gravitational and electromagnetic forces can be considered in function of the particular scenario of modelling. In this article, external forces are neglected.

Taking into account that inertia is neglected, forces balance on each bead i writes:

$$\mathbf{F}_i^{(h)} + \mathbf{F}_i^{(\lambda)} + \mathbf{F}_i^{(\phi)} + \mathbf{F}_i^{(b)'} + \mathbf{F}_i^{(e)} = \mathbf{0} \tag{81}$$

Given the definition of the hydrodynamic drag force, an explicit stochastic expression for the bead velocity can be obtained:

$$\frac{d\mathbf{r}_i}{dt} = \left[\kappa(\mathbf{r}_i)\cdot\mathbf{r}_i\right] - \frac{1}{\zeta}\left\{\left(\sum_{j=1}^{n-1}\mathbf{n}_{ij}\lambda_j\right) + \mathbf{F}_i^{(\phi)} + \mathbf{F}_i^{(b)'} + \mathbf{F}_i^{(e)}\right\} \tag{82}$$

Geometrical projected random forces guarantee the inextensibility condition when no external fields are imposed. In other scenario, constraints on the rod lengths have to be considered. For instance, in a Cartesian coordinates system we have:

$$0 = \sum_{i=1}^{n}\dot{\mathbf{r}}_i\cdot\mathbf{n}_{ij} \quad \text{for } j = 1,\ldots,n-1 \tag{83}$$

Putting together Eqs. (82) and (83) a linear system of equations describing the kinematics of a non-freely-jointed multi-bead-rod model is constituted, where the unknown variables are n bead velocities $\dot{\mathbf{r}}_i$ and $n-1$ rod tensions λ_j.

4.2 Integration Schemes

Several numerical integration schemes have been proposed to integrate the differential stochastic equation equivalent to the FP equation given by Curtiss for the general multi-bead-rod chain in both generalized coordinate systems and Cartesian reference systems. In the case of generalized coordinates, the task is feasible if the number of degrees of freedom is small, otherwise the numerical complexity makes this option impractical [3]. Some simulations at equilibrium using a numerical integration in generalized coordinates were made by Pear and Weiner [5, 81]. The possibilities for integrating numerically in a Cartesian space are more varied and, in principle, the numerical methods employed for the bead-spring models are applicable, but additional controls are required for satisfying the constraints rigorously, specially in simulations for large time intervals [3].

Another integration numerical method for systems including constraints was given by Allison and McCammon under the name of SHAKE-HI algorithm [91]. In the general form of the algorithm, bead positions are calculated in two steps: an unconstrained step followed by a constrained one. Two particular versions of the SHAKE-HI algorithm are the most cited numerical schemes employed to integrate the differential stochastic equation for a multi-bead-rod model in a Cartesian space: the mid-point stepping scheme proposed by Fixman [82, 85] and the predictor-corrector scheme developed by Liu [63, 76].

4.2.1 Mid-Point Algorithm

In 1978 Ermak and McCammon showed that the gradient of the diffusivity must to be incorporated into a BD algorithm when the bead diffusivity depends on the configuration of the Brownian system [92]. It has been shown that the diffusivity of a multi-bead-rod chain is variable because of the presence of rigid constraints and, also, as consequence of considering hydrodynamic interaction [85]. A clever way to counteract the wrong drift produced by the variable diffusivity in a BD algorithm was proposed by Fixman [82]. He suggested employing a second-order time step to integrate the stochastic differential equation. In fact, any higher order time step is able to handle correctly the variable diffusivity. In this numerical algorithm the use of potential metric forces $\mathbf{F}_i^{(m)}$ is required and has to be added to the left term of Eq. (81). In brief, potential metric forces are function of the constrained configuration of the chain. Extended descriptions and detailed definitions for this “extra” metric force can be found elsewhere [3, 84, 89]. From a global point of view, this algorithm is able to deal with hydrodynamic interaction and anisotropic friction tensors. For the particular multi-bead-rod chain model presented in this work, the differential stochastic equation required for the mid-step scheme writes as follows:

$$\dot{\mathbf{r}}_i = \frac{1}{\zeta}\left(\mathbf{F}_i^{(\lambda)} + \mathbf{F}_i^{(uc)} + \mathbf{F}_i^{(b)'}\right) \tag{84}$$

where $\mathbf{F}_i^{(uc)} = \zeta[\boldsymbol{\kappa}(\mathbf{r}_i)\cdot\mathbf{r}_i] + \mathbf{F}_i^{(\phi)} + \mathbf{F}_i^{(e)} + \mathbf{F}_i^{(m)}$. Keeping in mind that hydrodynamic interaction is neglected and an isotropic friction tensor is supposed, then a single time step $[t,\, t+\Delta t]$ for the mid-step algorithm is constituted by the following sub-steps:

1. Generation of geometrical projected random forces at the beginning of the time step $\mathbf{F}_i^{(b)'}(t)$ following the complete algorithm describe by Hinch and co-workers [84–86].
2. Calculate the mid-step position as follows:

$$\mathbf{r}_i\left(t+\frac{\Delta t}{2}\right) = \mathbf{r}_i(t) + \dot{\mathbf{r}}_i(t)\frac{\Delta t}{2} \tag{85}$$

   where the initial-step velocity $\dot{\mathbf{r}}_i(t)$ is calculated neglecting the constraints on the rod lengths:

$$\dot{\mathbf{r}}_i(t) = \frac{1}{\zeta}\left(\mathbf{F}_i^{(uc)}(t) + \mathbf{F}_i^{(b)'}(t)\right) \tag{86}$$

3. Calculate the end-step position by using the next equation:

$$\mathbf{r}_i(t+\Delta t) = \mathbf{r}_i(t) + \dot{\mathbf{r}}_i(*)\Delta t \tag{87}$$

   where the mid-step velocity is obtained from the solution of the linear system:

$$\dot{\mathbf{r}}_i(*) = \frac{1}{\zeta}\left[\mathbf{F}_i^{(\lambda)}\left(t+\frac{\Delta t}{2}\right) + \mathbf{F}_i^{(uc)}\left(t+\frac{\Delta t}{2}\right) + \mathbf{F}_i^{(b)'}(t)\right] \tag{88}$$

$$0 = \sum_{i=1}^{n} \dot{\mathbf{r}}_i(*) \cdot \mathbf{n}_{ij}\left(t + \frac{\Delta t}{2}\right) \tag{89}$$

where $\dot{\mathbf{r}}_i(*)$ is the constrained bead velocity at the mid-step, but calculated with the random stochastic forces generated at the beginning of the time step. This procedure is coherent with the Stratonovich interpretation of the stochastic random forces [3, 93]. This algorithm does not guarantee an invariable rod length at the end of the time step, for that reason a truncation error is employed. Once the rod length at the end of a given time step exceeds certain tolerance, the inter-bead distances are reset to the constant value, conserving the rod orientations.

4.2.2 *Predictor-Corrector Scheme*

The predictor-corrector scheme is a singular and limiting case of the SHAKE-HI algorithm. One can say that is singular because it requires absolutely neglecting the hydrodynamic interaction and dealing with an isotropic friction tensor. On the other hand, this algorithm is limiting because the two-step procedure is merged in an iterative single-step. The predictor-corrector scheme was employed by Liu for simulating the dynamics of a Kramers chain submitted to steady potential flows [76]. Doyle demonstrated that both the predictor-corrector scheme and the Fixman's mid-step algorithm generate the same trajectories for a dilute Kramers bead-rod chain with an isotropic friction tensor and in absence of hydrodynamic interaction [93]. It is emphasized that neglecting the hydrodynamic interactions, supposing an isotropic friction tensor and employing this limiting case of the SHAKE-HI algorithm are necessary conditions for eliminating the metric potential forces from the differential stochastic equation in Cartesian coordinates without incurring in deviations from the FP equation for the multi-bead-rod model [3].

For a time step $[t,\ t + \Delta t]$, displacement of bead i is obtained in two stages. The first one, called predictor step, is given by an unconstrained movement:

$$\mathbf{r}_i^*(t + \Delta t) = \mathbf{r}_i(t) + \dot{\mathbf{r}}_i(t)\Delta t \tag{90}$$

where

$$\dot{\mathbf{r}}_i(t) = \frac{1}{\zeta}\left(\mathbf{F}_i^{(uc)}(t) + \mathbf{F}_i^{(b)'}(t)\right) \quad \text{and}$$

$$\mathbf{F}_i^{(uc)} = \zeta\left[\boldsymbol{\kappa}(\mathbf{r}_i) \cdot \mathbf{r}_i\right] + \mathbf{F}_i^{(\phi)} + \mathbf{F}_i^{(e)}.$$

Subsequently, an iterative corrector step is required for taking into account the inextensibility of rods:

$$\mathbf{r}_i(t + \Delta t) = \mathbf{r}_i^*(t + \Delta t) + \frac{1}{\zeta}\mathbf{F}_i^{(\lambda)}\Delta t \tag{91}$$

where $\mathbf{F}_i^{(\lambda)}$ is given by Eq. (69). The Lagrange multipliers λ_i are calculated so that inter-bead distances are satisfied within a certain tolerance:

$$\left(\mathbf{r}_{i+1}(t + \Delta t) - \mathbf{r}_i(t + \Delta t)\right)^2 - a^2 = \varepsilon^2 \tag{92}$$

Combining Eqs. (91) and (92), a system of quadratic equations for λ_i is generated. This system has the general form:

$$\begin{aligned}\frac{2\Delta t}{\zeta}\mathbf{b}_i \cdot \left(\lambda_{i-1}^{[n]}\mathbf{u}_{i-1} - 2\lambda_i^{[n]}\mathbf{u}_i + \lambda_{i+1}^{[n]}\mathbf{u}_{i+1}\right) \\ = a^2 + \varepsilon^2 - \mathbf{b}_i \cdot \mathbf{b}_i - \left(\frac{\Delta t}{\zeta}\right)^2 \left(\lambda_{i-1}^{[n-1]}\mathbf{u}_{i-1}\right. \\ \left. - 2\lambda_i^{[n-1]}\mathbf{u}_i + \lambda_{i+1}^{[n-1]}\mathbf{u}_{i+1}\right)^2\end{aligned} \tag{93}$$

where $\mathbf{b}_i = \mathbf{r}_{i+1}^* - \mathbf{r}_i^*$ and $\lambda_i^{[n]}$ is the nth approximation of the Lagrange multiplier associated to rod i. Previous set of non-linear equations can be solved iteratively by a Picard's method by supposing the non-linear term (last term on the right-hand side) to be small in comparison with the linear terms (left-hand side). The iterative procedure is initiated with $\lambda_i^{[0]} = 0$ and is executed until the constraints are satisfied with regard to a certain truncation error ε^2. Once the iterative procedure has finished, the bead positions at the end of the time step are corrected using Eq. (91).

Additional to the Picard's method invoked to solve Eq. (93), an iterative Newton's method can converge faster than the Picard's one, but involving the calculation of a Jacobian matrix every time step [63].

4.3 Stress Tensor Calculation

From a formal point of view, deduction of a stress formula for bead-rod chains is not as straightforward as in the case of bead-spring models, where the physical configuration is an intimate reflect of the instantaneous mechanical state of the system. In the case of bead-rod chains, the pictorial arguments used for the bead-spring models are not enough and, in consequence, a deeper physical explanation is required.

There is a general consensus accepting that the modified Kramers expression (Eq. (46)) accounts for the contribution to the total shear stress coming from a diluted model system whose total change in momentum can be discretized on certain points, as is the case for a general bead-rod-spring model. A detailed derivation of this stress tensor formula using a general *phase-space* kinetic theory can be examined in Chaps. 17 and 18 of [28].

Care must be taken also when calculating numerically the stress tensor for systems containing constraints. Given the numerical singularities originated by the presence of constraints, one is particularly interested in the correct implementation of a stress tensor formula into the BD algorithm.

It is found that a correct estimation of the stress tensor must to be closely linked to the integration scheme used in the simulation.

In order to account rigorously for the Brownian effects on the stress tensor, the algorithm estimating the stress tensor must to consider the discontinuity of the Brownian forces during a given time step [86, 93], specially when no-flow conditions are being simulated. To do this, the modified Kramers formula has to be interpreted as an average in time. For a mid-step algorithm, for example, the average has to be carried out using the beginning and the end of the time step [94]:

$$\boldsymbol{\tau}_p(t) = \frac{c}{2}\sum_{v=1}^{n}\Big\langle \mathbf{R}_v(t)\otimes\mathbf{F}_v^{(h)}(t) + \mathbf{R}_v(t+\Delta t)\otimes\mathbf{F}_v^{(h)}(t+\Delta t)\Big\rangle \tag{94}$$

Doyle demonstrated that two iterations of the predictor-corrector scheme producing an increment of Δt are equivalent to one time-step of the mid-step algorithm [93]. Based on the previous fact, it can be easily showed that Eq. (94) is also a correct interpretation of the virial tensor for the predictor-corrector algorithm.

An alternative way to correctly account for the Brownian contribution in a first order integration scheme (as the predictor-corrector algorithm), considering a “long-lasting” action of the random forces, can be envisaged using the next algorithm:

1. Update the bead-rod position by executing one explicit time step from t to $t+\Delta t$.
2. Using the same Brownian forces used at time t, recalculation of the hydrodynamic drag forces $\tilde{\mathbf{F}}_v^{(h)}(t+\Delta t)$ with the updated configuration at $t+\Delta t$.
3. Determination of the shear-stress tensor at time t by computing:

$$\boldsymbol{\tau}_p(t) = c\sum_{v}\Big\langle \mathbf{R}_v(t+\Delta t)\otimes\tilde{\mathbf{F}}_v^{(h)}(t+\Delta t)\Big\rangle \tag{95}$$

In previous algorithm Brownian forces are interpreted in the Stratonovich sense, which is equivalent to stating that the stochastic forcing occurs throughout the entire time step [93]. This interpretation of the Brownian forces is particularly important in the systems containing constraints because has direct consequences in both integration schemes (as observed clearly in the mid-step algorithm) and stress tensor calculations. A simple example showing the impact of the interpretation of the Brownian nature in the shear-stress tensor calculation is given next. Consider a diluted 2D fibre aligned with the x axis at time t as show in Fig. 17. Friction acting on beads is supposed isotropic. No external flow is considered, only Brownian and drag forces take place.

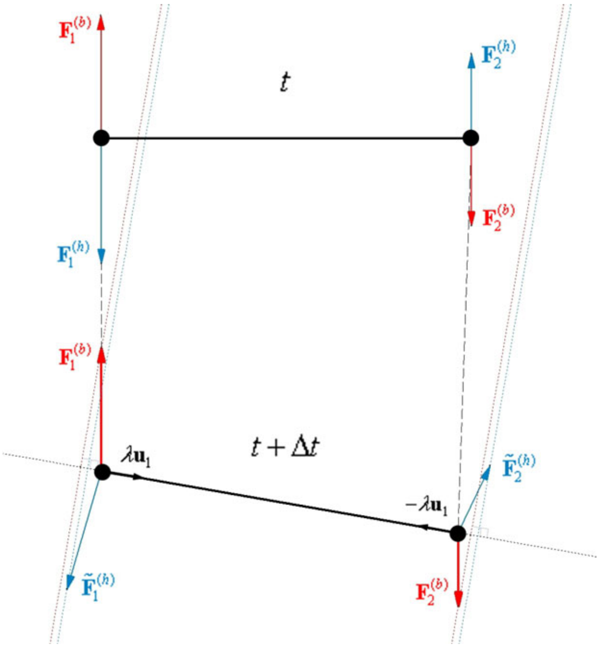

Fig. 17 Example of the “long-lasting” action of Brownian forces over a quiescent 2D single rod throughout a time step. An isotropic friction coefficient is supposed. *Upper rod* corresponds to the configuration at time t, *lower rod* corresponds to the configuration at time $t+\Delta t$. Observe that hydrodynamic forces at the end of the time step present non-null projections on the fibre axis

It can be easily demonstrated, from the example of the geometrical projection of Brownian forces given in Sect. 4.1, that effective random forces in such configuration only occurs perpendicularly to the fibre axis, explaining why Brownian forces depicted in Fig. 17 at time t are perpendicular to fibre axis. If Brownian forces acting at time t are interpreted as instantaneous and stress tensor calculation is based exclusively on the mechanical balance obtained at time t then the contribution of the fibre to the shear-stress tensor would be null ($\tau_p = \mathbf{0}$), as hydrodynamic forces $\mathbf{F}_v^{(h)}(t)$ are always perpendicular to the connector vectors $\mathbf{R}_v(t)$.

Suppose now that Brownian forces at time t occurs continuously until the end of the time step $t+\Delta t$ as showed in Fig. 17, where Brownian forces conserve magnitude and direction for the updated fibre configuration at time $t+\Delta t$. In that case, the contribution of the fibre to the shear-stress must include the configuration and mechanical balance of the fibre at the end of the time step. By employing the “long-lasting” Brownian forces algorithm, the shear-stress tensor contribution of a representative ensemble of fibres initially aligned with the x axis converges to the next form:

$$\boldsymbol{\tau}_p = \alpha\begin{pmatrix}1 & 0\\ 0 & -1\end{pmatrix} \tag{96}$$

where α is a constant function of the temperature. Previous shear-stress tensor is in coherence with the results in theoretical mechanics for a quiescent rigid fibre immersed in a

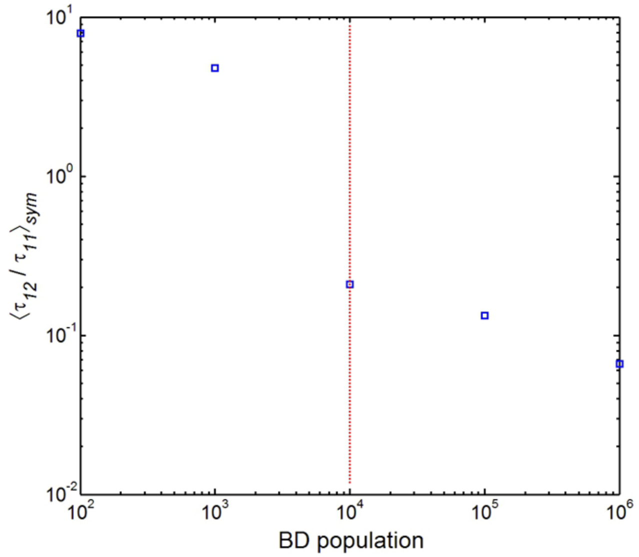

Fig. 18 Ratio between the out-of-diagonal and diagonal components of the first time step shear-stress tensor in function of the BD population of 2D rigid-fibres initially aligned with the x axis. Shear-stress tensor has been made symmetrical by Eq. (97). *Vertical dotted line* marks the minimum required population for obtaining acceptable convergence to the central values in absence of external flow. Consider that in the current case the ratio $\langle \tau_{12}/\tau_{11} \rangle_{\mathrm{sym}}$ is theoretically equal to zero

solvent, in which fibre experiences tension along its axis and compression in the normal direction.

Symmetry is another important issue when using the Kramers-Kirkwood expression for estimating the contribution of a given micro-mechanical model to the shear-stress tensor. Diluted bead-rod chains submitted to a homogeneous velocity field, in absence of external forces $\mathbf{F}_v^{(e)}$, are intended to produce a symmetric contribution to the total shear-stress. In a BD approach, symmetry is reached from the average of progressively bigger populations of bead-rod chains and/or the use of improved random number generators. In our BD simulation, limited by the size of the BD system, the estimated shear-stress tensor at each time $\tau_p(t)$, is made symmetrical in order to calculate the rheological properties following the next formula:

$$[\boldsymbol{\tau}_p(t)]_{\mathrm{sym}} = \frac{1}{2}\left([\boldsymbol{\tau}_p(t)] + [\boldsymbol{\tau}_p(t)]^T\right) \tag{97}$$

As expected, convergence of the previous expression to the central values of shear-stress strongly depends on the size of the BD population. For example, considering the 2D rigid-fibre aligned with the x axis presented previously, in Fig. 18 the progressively convergence of the out-of-diagonal component of the shear-stress tensor can be appreciated as the size of the BD population is increased.

Notice that, in absence of flow, at least a population of 10^4 systems is required to converge to the central values. Otherwise, aberrant values for the out-of-diagonal component of the shear-stress tensor can be obtained.

4.4 The Trimer Chain

In order to study the generalities of the BD simulations for multi-bead-rod models it was decided to use the freely-jointed (three-beads)–(two-rods) model, also known as the *trumbbell* or *trimer* system. This model is composed of three beads with isotropic friction coefficient ζ connected by two freely jointed rigid mass-less rods of length a. Hydrodynamic interaction is neglected.

Trimer chain is a better testing model than the rigid dumbbell because a more rigorously evaluation of the integration algorithms can be carried out given the presence of two adjacent constraints. On the other hand, an exact numerical expression for the dynamic response of a dilute solution of *trimer* systems was obtained separately by Fixman and Hassager [77, 95]. This numerical solution is in coherence with the FP equation for a multi-bead-rod chain in polymer kinetic theory [28, 67], actually deviated from that one for multi-bead-spring chains [80]. In the Hassager's solution, dynamic modulus of the *trimer* system is described using four relaxation times λ_i^H of which the longest one writes:

$$\lambda_1^H = \frac{\zeta a^2}{5.4376 k_B T} \tag{98}$$

With the aim to compare properly with the BD predictions, time scales for the theoretical data are rescaled using λ_1^H.

In a *trimer* chain hydrodynamic interaction is neglected and friction is supposed isotropic. For that reason, a first-order integration scheme in coherence with the predictor corrector algorithm can be implemented in the BD simulation of *trimer* chains avoiding the use of metric potential forces. In this paper, shear-stress tensor contribution is estimated with the modified Kramers-Kirkwood expression using the "long-lasting" Brownian forces algorithm. From now on, bi-dimensional BD simulations are implemented because we have found that this modelling correctly approaches the analytic solution of the FP equation for a *trimer* system. Time scale in the BD simulations is made dimensionless using the longest relaxation time (or rotational diffusion time) of an equal-length (n-bead)–(rigid-rod) system given by [28]:

$$\lambda_n = \frac{\zeta L^2 n(n+1)}{72(n-1) k_B T} \tag{99}$$

where $L = a(n-1)$. It means that for a *trimer* system, where $n = 3$, time is scaled using $\lambda_3 = \zeta a^2 / 3 k_B T$. Time step, instead, needs to be scaled with regard to the shortest relaxation time; bead diffusion time is normally employed, $\lambda_{\mathrm{bead}} = \zeta a^2 / k_B T$.

As showed in the analysis of the Hookean-dumbbell model (Sect. 3.4.1), the BD considerations when estimating

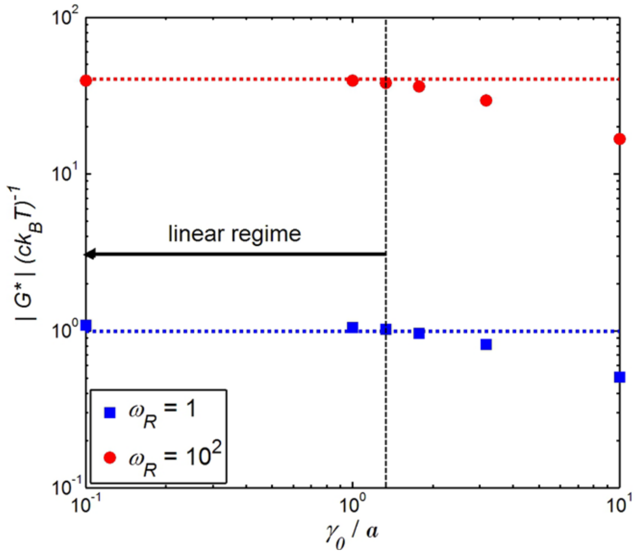

Fig. 19 Identification of the limit of the linear viscoelastic regime for a dilute suspension of *trimers* by BD simulation. Absolute value of the complex modulus in function of the maximal deformation applied for two reduced frequencies: $\omega_R = 1$ and $\omega_R = 10^2$. *Horizontal dotted lines* correspond to the theoretical values calculated by Hassager. *Dashed vertical line* marks the limit of the linear viscoelastic regime

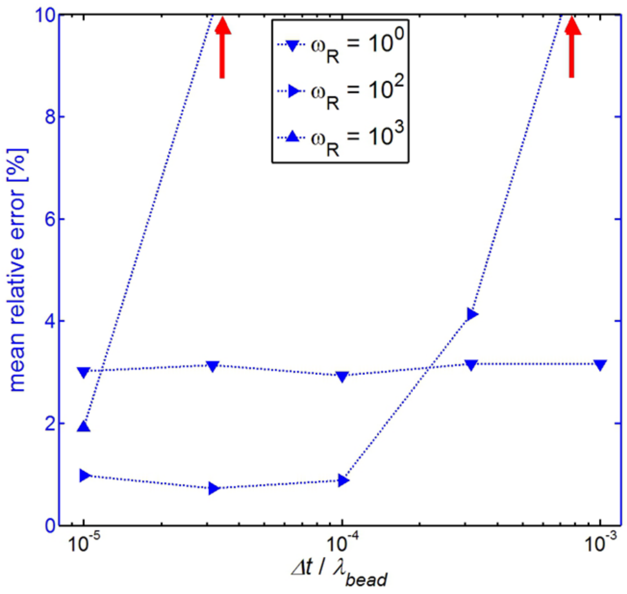

Fig. 20 Mean relative error of the BD prediction of the complex modulus for a *trimer* system in function of the time step. Mean relative error is the average of the relative errors for storage and loss modules. Relative error is defined as follows: $|(\log G'_{\mathrm{BD}}(\omega_R) - \log G'_{th}(\omega_R))/\log \Theta|$, where $\Theta = G''_{th}(\omega_R = 10^3)/G'_{th}(\omega_R = 1)$ is the maximal interval of complex modulus variation in the tested frequency interval. A population of 10^4 *trimers* has been employed

the equilibrium properties (in absence of flow) are analogues to those ones obtained under linear dynamic solicitation at the characteristic frequency, i.e. at $\omega_R = 1$. For that reason, no-flow properties are skipped and linear dynamic response of the system is studied directly.

BD simulations of the small-amplitude oscillatory deformation tests are carried out according to the algorithm explained in Sect. 2. First of all, the limit of the linear viscoelastic regime needs to be determined. In order to extract this information from the BD simulations, the norm of the complex modulus at the characteristic frequency is plotted in function of the maximal applied strain. In order to marginalize the numerical issues of the BD simulation, a population of 10^4 chains and a time step equivalent to $\lambda_{\text{bead}}/10^5$ are employed.

Figure 19 shows that the limit of the linear viscoelastic regime for a dilute solution of *trimer* systems corresponds to a maximal deformation $\gamma_0 \approx 1.33a$. At lower values, dynamic moduli obtained by BD simulations are independent of the maximal deformation imposed. On the other hand, Fig. 19 evidences that multi-bead-rod models exhibit a shear-thinning behavior, contrary to the multi-bead-spring counterparts. Using a constant BD population (10^4 *trimers*) and a constant time step ($\lambda_{\text{bead}}/10^5$), computational time (2× Quad-Core AMD Opteron™ 2376 (2300 MHz)) employed to predict the complex modulus at $\omega_R = 1$ was found 8.7 times longer than the computational time used at $\omega_R = 10^2$. This fact is explained by the higher number of time steps required at low frequencies for sweeping one-and-a-half period of oscillation and determining the maximal shear-stress and phase angle between strain and stress signals.

In the current BD approach, a first-order integration scheme was implemented and, therefore, time step strongly influences the convergence of the simulation towards the central values. In Fig. 20 the effect of the time step on the convergence of the BD simulation is presented (from now on, imposed maximal deformation is chosen inside the linear viscoelastic regime). 10^4 *trimers* were employed as BD system in order to reduce the distortions coming from the random number generation. Convergence of the BD simulation is tested in three different flow scenarios: $\omega_R = 1$, which is representative of the thermal-to-flow induced transition, $\omega_R = 10^2$, which is characteristic of the mild flow-induced regime, and, $\omega_R = 10^3$, which is typical of a strongly flow-induced regime.

In Fig. 20 is clearly observed the strong influence of the length of the time step in the convergence of the explicit integration scheme at high frequencies. At low frequencies ($\omega_R = 1$), characteristic of the thermal-induced regime, BD performance (relative error ∼ 3 %) is nearly independent of the length of the time step. In this regime, convergence of the integration scheme is guaranteed with a time step equal to $\lambda_{\text{bead}} \cdot 10^{-3}$. Error obtained at this flow regime is mainly coming from the random number generation algorithm; implementation of a more sophisticated generator is necessary to reduce this noise. When increasing the frequency, BD

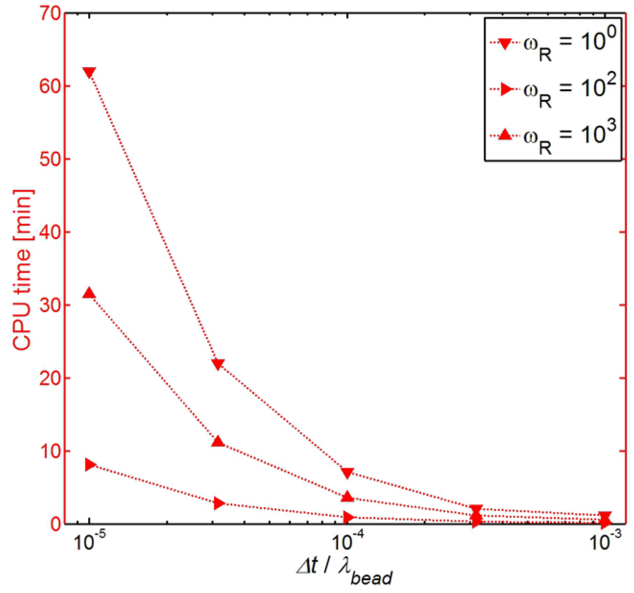

Fig. 21 CPU time required to predict complex modulus for a *trimer* system at three different frequencies ($\omega_R = 1$, $\omega_R = 10^2$ and $\omega_R = 10^3$) in function of the time step. A population of 10^4 *trimers* has been employed

performance is progressively more affected by the integration scheme. As showed for the multi-bead-spring models, at higher frequencies than the characteristic one, the flow-induced forces control the kinematics of the system; for that reason, higher velocities require smaller time steps in order to guarantee a correct numerical integration. This fact is clearly captured in Fig. 20: in the mild flow-induced regime, i.e. $\omega_R = 10^2$, mean relative error of the BD prediction goes from 1 % to 12 % when the length of the time step is enlarged from $\lambda_{\text{bead}} \cdot 10^{-5}$ to $\lambda_{\text{bead}} \cdot 10^{-3}$. In the case of strong flow-induced regime, i.e. $\omega_R = 10^3$, mean relative error of the BD prediction explodes from 2 % to more than 20 % when the length of the time step is augmented just in one-half order of magnitude from $\lambda_{\text{bead}} \cdot 10^{-5}$.

On the other hand, in Fig. 21 is observed that simulation time is reduced as length of the time step is enlarged. Moreover, for a given value of time step, computational time used for calculating complex modulus strongly depends on the tested frequency; for instance, when implementing $\Delta t = \lambda_{\text{bead}} \cdot 10^{-5}$, simulations last in minutes 62.0, 8.1 and 31.5 for reduced frequencies of 1, 10^2 and 10^3 respectively. Simulation at the characteristic frequency has the biggest computational cost because it requires the longest analytical step (1.5 periods of oscillatory deformation at the lowest frequency). Moreover, simulation at the highest frequency is also time-consuming because an additional refining of the nominal time step is required for well describe the oscillatory deformation signal.

In what follows, an extended sweep test over 21 frequencies homogeneously distributed within an interval of reduced frequencies going from 10^{-2} to 10^3 was used to evaluate the global performance of the implemented BD simulation predicting the linear dynamic response of a *trimer* system in dilute solution. A time step equal to $\lambda_{\text{bead}} \cdot 10^{-5}$ has been employed to guarantee the best convergence of the integration scheme inside the simulated frequency range. In Fig. 22 the Hassager's numerical solution is compared with the BD predictions for the frequency sweep test. Hassager's complex modulus is presented in a reduced frequency scale $\omega_R = \omega\lambda_1^H$, and BD results are plotted in a reduced frequency scale $\omega_R = \omega\lambda_3$, where λ_3 is the rotational diffusion time for a (3-beads)–(rigid-rod) system of equal length.

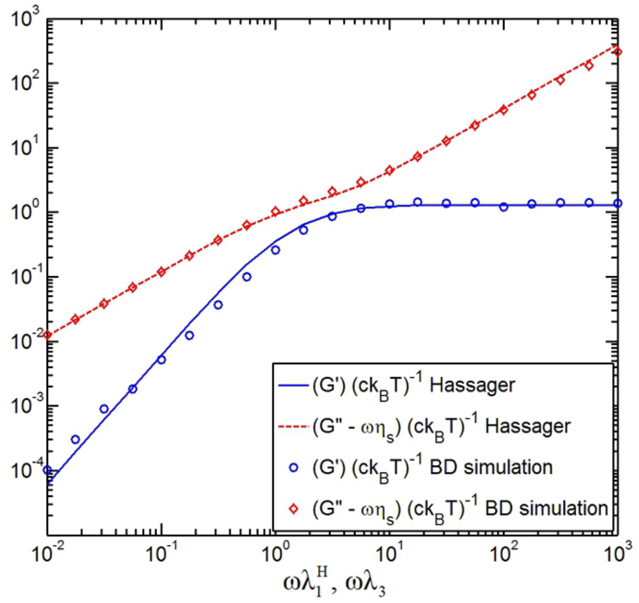

Fig. 22 Dynamic modulus of a freely jointed (three-beads)–(two-rods) system in a proper reduced frequency scale: comparison between the Hassager's numerical solution and the current BD simulation. λ_1^H is the main relaxation time in the Hassager's solution and λ_3 is the rotational diffusion time of a system composed of (3-beads)–(rigid-rod) with equal length. a and ζ are fixed to 1, ck_BT to 0.1 and K_b to 0 in a consistent system of units

BD algorithm yielded a complex modulus in good agreement with the Hassager's numerical solution of the *trimer* system as observed in Fig. 22. On the other hand, this large-sweep simulation demonstrated that a bi-dimensional modelling is able to correctly approach the 3D analytical solution given by Hassager and, therefore, avoids implementing a three-dimensional modelling, which would be more expensive in computational time. Two different regions are clearly differentiated in the dynamic response of a *trimer* system: a low frequency regime exhibiting a typical Maxwell terminal behavior, where the thermal activity (or Brownian forces) drives the kinematic of the system; and a high frequency regime, where the domination of flow forces over the diffusivity terms produces a plateau for the storage modulus and a limiting constant viscosity $(G(\omega)/\omega) - \eta_s$ larger than

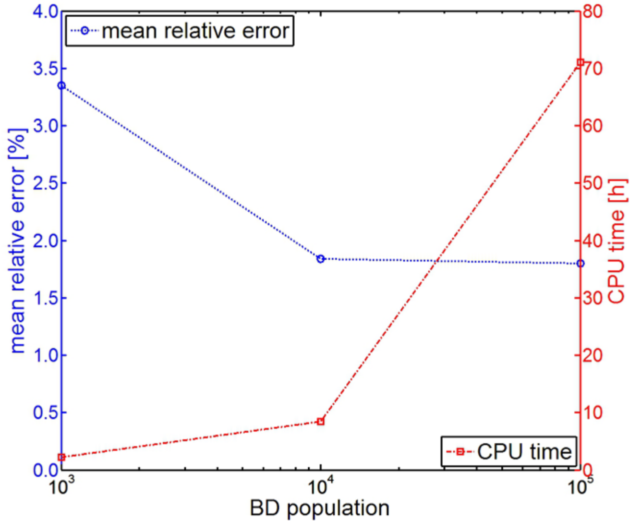

Fig. 23 Mean relative error of the storage modulus prediction (for a *trimer* system) and total computational time in function of the BD population. Mean relative errors are calculated as the average of 17 points distributed homogeneously in a reduced frequency range going from 10^{-2} to 10^2. Relative error is calculated as follows: $|(\log G'_{\mathrm{BD}}(\omega_R) - \log G'_{th}(\omega_R))/\log \Theta|$, where $\Theta = G''_{th}(\omega_R = 10^2)/G'_{th}(\omega_R = 10^{-2})$ is the maximal interval of complex modulus variation in the tested frequency interval

zero. The existence of a non-zero limiting viscosity is physically more coherent than the classical responses of multi-bead-spring chains, where the contribution to the dynamic viscosity disappears at high frequencies.

As already mentioned in the section devoted to the bead-spring models, the number of entities (or trajectories) plays a fundamental role in the performance of the BD simulations. Performance of the global simulation in function of the BD population is presented in Fig. 23. The performance of the BD simulation is measured in terms of the mean of the relative errors for 17 storage modulus values homogeneously distributed in an interval of reduced frequencies going from 10^{-2} to 10^2. Loss modulus signature was found practically insensitive to the BD population; mean relative error for the loss modulus signal was equal to 0.3 %.

As expected, a linear evolution of the computational time (2× Quad-Core AMD Opteron™ 2376 (2300 MHz)) in function of the number of *trimers* simulated is checked. It was corroborated that a population of 10^4 systems guarantees a good compromise between computational time and rheological prediction performance.

4.5 Non-freely-Jointed Chains (and Non-straight Natural Configurations)

Bending potential defined in Eq. (71) is based on the worm-like chain continuous model. It this model, the equilibrium configuration corresponds to a perfectly straight chain. This fact means that the minimum value of the internal bending energy is associated with a multi-bead-rod chain whose unitary rod vectors $\mathbf{u}_j$ are all the same. Bending potential force acting on bead k can be easily deduced as the derivative of the discrete bending potential with respect to the position of bead k (Eq. (72)). Total bending force acting on bead k only depends on the local chain configuration and can be interpreted as the sum of independent contributions coming from all the two-rod sub-sections containing bead k. Demonstration of the previous can be found elsewhere [27].

However, finite-contour-length high-aspect-ratio systems with naturally non-straight configurations at equilibrium can be found in the physical world (for example carbon nanotubes, rod-like virus, genes) and, therefore, a redefinition of the discrete bending potential taking into account a natural non-straight configuration is required to simulate the dynamic response of naturally bent structures.

In this context, a suitable redefinition of the discrete bending potential for a multi-bead-rod model with a naturally bent configuration at equilibrium can be expressed in the next way:

$$\phi = -\frac{K_b}{a}\sum_{i=2}^{n-1} \mathbf{Z}_i \mathbf{u}_i \cdot \mathbf{u}_{i-1} = -\frac{K_b}{a}\sum_{i=2}^{n-1} \mathbf{u}'_i \cdot \mathbf{u}_{i-1} \tag{100}$$

where $\mathbf{Z}_i$ is a linear operator that counter-rotates vector $\mathbf{u}_i$ of $\Delta\theta^0_{i,i-1}$ (interior angle between $\mathbf{u}_i$ and $\mathbf{u}_{i-1}$ at the equilibrium configuration) and $\mathbf{u}'_i$ is the rotated vector $\mathbf{Z}_i\mathbf{u}_i$. In an analogous way with the straight case, bending force coming from the potential in Eq. (100) takes the next form:

$$\mathbf{F}^{\phi}_k = -\frac{\partial \phi}{\partial \mathbf{r}_k} = \frac{K_b}{a}\sum_{i=2}^{n-1} \frac{\partial(\mathbf{u}'_i \cdot \mathbf{u}_{i-1})}{\partial \mathbf{r}_k} \tag{101}$$

Considering that the total bending force in Eq. (101) can also be interpreted as the sum of independent contributions coming from all the two-rod sub-sections containing bead k, as shown in [27], next algorithm is proposed for computing the total bending forces in coherence with a naturally bent configuration:

1. Decomposition of the multi-bead-rod (n beads) system into $n-2$ sub-section of two consecutive rods as shown in Fig. 24 (note that sub-section p is composed by beads p, $p+1$ and $p+2$).
2. Calculation of the non-zero contributions to the bending forces over all beads composing each sub-section p as follows:
   - Bending force on bead p of sub-section p as:

$$\mathbf{F}^{(\phi)}_{p,p} = -\frac{K_b}{a^2}(\boldsymbol{\delta} - \mathbf{u}_p \otimes \mathbf{u}_p)\cdot \mathbf{u}'_{p+1} \tag{102}$$

   - Bending force on bead $p+2$ of sub-section p as:

$$\mathbf{F}^{\phi}_{p+2,p} = \mathbf{Z}^{-1}_{p+1}\cdot\left[\frac{K_b}{a^2}(\boldsymbol{\delta} - \mathbf{u}'_{p+1} \otimes \mathbf{u}'_{p+1})\cdot \mathbf{u}_p\right] \tag{103}$$

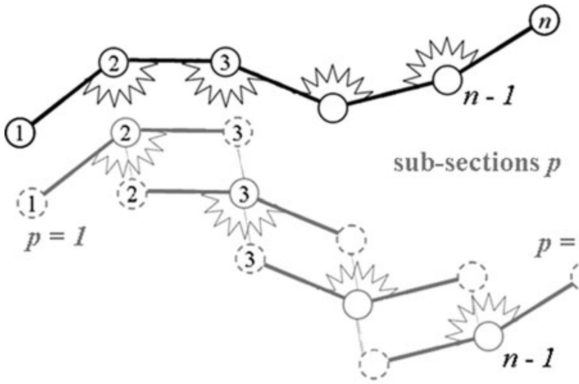

Fig. 24 Multi-bead-rod model of n beads (in *black*) decomposed in $n-2$ sub-sections p constituted by two consecutive rods (in *gray*)

Bending force on bead $p+2$ of sub-section p has been rotated back (operator $\mathbf{Z}_{p+1}^{-1}$) in order to correct the direction of the force, that must to be in coherence with the actual bent configuration.

- As the bending potential in each sub-section is locally independent of the adjacent sub-sections, it must to satisfy mechanical equilibrium and, hence, bending force on bead $p+1$ of sub-section p writes:

$$\mathbf{F}_{p+1,p}^{(\phi)} = -\mathbf{F}_{p,p}^{(\phi)} - \mathbf{F}_{p+2,p}^{(\phi)} \tag{104}$$

3. Finally, total bending force acting on bead k is calculated as follows:

$$\mathbf{F}_{k}^{(\phi)} = \sum_{p=1}^{n-2} \mathbf{F}_{k,p}^{(\phi)} \tag{105}$$

Given the previous more general definition of the bending forces for a multi-bead-rod model with any equilibrium configuration, we can deal with more scientific rigor the effects of the bending flexibility on the dynamic response of multi-bead-rod chains in dilute solution. To show this, bi-dimensional BD simulations are carried out for several non-freely-jointed (three-beads)–(two-rods) systems. In this case, hydrodynamic interaction is neglected and an isotropic friction tensor is supposed. Previous premises allowed us to implement a first-order integration scheme in coherence with the predictor-corrector algorithm; no metric potential forces are required in the formulation. Shear-stress tensor contribution coming from the bead-rod chains is calculated with the modified Kramers Kirkwood expression using the "long-lasting" Brownian forces algorithm.

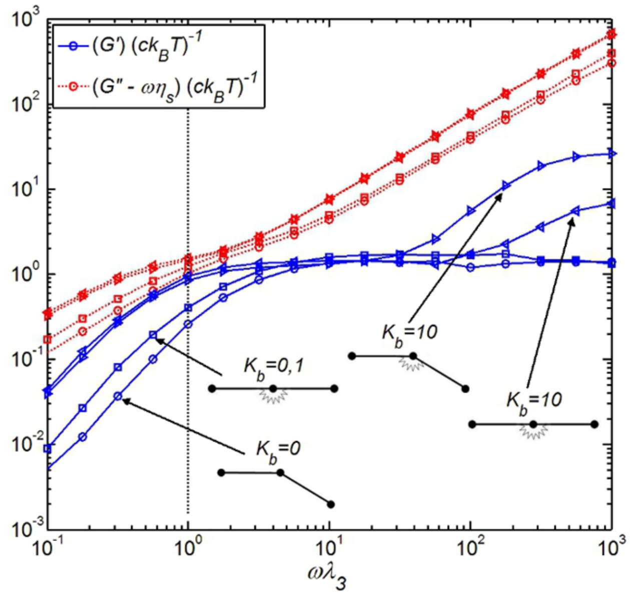

Fig. 25 BD predicted complex modulus of different (three-beads)–(two-rods) systems: *freely jointed*, *non-freely jointed* with natural straight configuration ($K_b = 0.1$ and $K_b = 10$ in a consistent system of units) and non-freely-jointed with natural bent configuration ($K_b = 10$ in a consistent system of units and $\Delta\theta^{\max} = 30°$). a and ζ are fixed to 1 and ck_BT to 0.1 in a consistent system of units. λ_3 is the rotational diffusion time of a (3-beads)–(rigid-rod) system of equal length

A large range of dynamic responses in linear viscoelasticity is deployed depending on the equilibrium configuration and the bending rigidity constant. To explain this, in Fig. 25 the dynamic responses of a freely-jointed system, two non-freely-jointed systems with natural straight configuration and a non-freely-jointed system with a naturally bent configuration are compared. Rod misalignment (i.e. the natural bent multi-bead-rod configuration) is generated following the next formula:

$$\theta_i^0 = \theta_{i-1}^0 - \Delta\theta^{\max} + \mathrm{U}(0,1)\cdot 2\Delta\theta^{\max} \tag{106}$$

where θ_i^0 is the equilibrium director angle of rod i, $\Delta\theta^{\max}$ is the maximal misalignment between two consecutive rods and $\mathrm{U}(0,1)$ is a continuous uniform random distribution function defined between 0 and 1.

In a general way, when the bending rigidity constant K_b is equal or greater than the thermal coefficient ak_BT, the loss modulus is enhanced over the entire frequency range and the storage modulus is increased in the low frequency regime. Otherwise, if the bending rigidity constant is much lower than the thermal coefficient ($K_b \ll ak_BT$), a dynamic response similar to that one of a freely jointed system is obtained, showing just one dominant relaxation time associated with the thermal-to-flow induced motion transition.

Additionally, in Fig. 25 the apparition of new relaxation processes when the bending rigidity constant is considerably greater than the thermal coefficient (i.e. $K_b \gg ak_BT$) is observed. For instance, the activation of a mild elasticity at intermediate frequencies is clearly noticed in the dynamic response of the non-freely jointed (three-beads)–(two-rods) system with bending rigidity constant $K_b = 10$. When comparing the straight configuration with the bent one, even

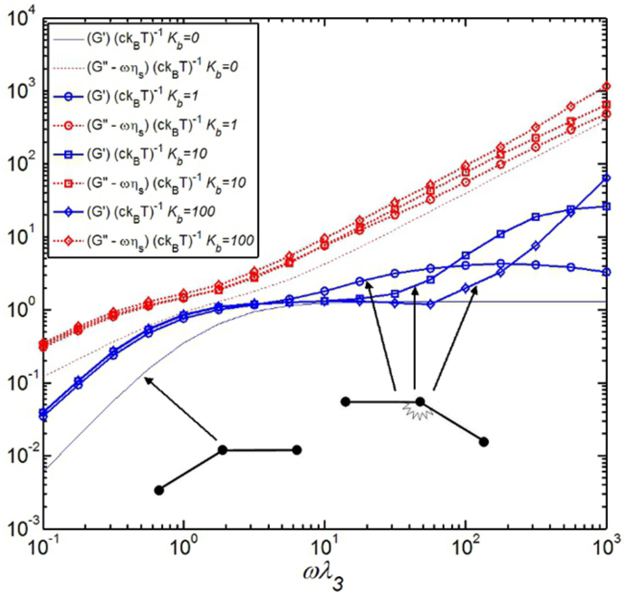

Fig. 26 BD predicted complex modulus of a non-freely jointed (three-beads)–(two-rods) system with a natural bent configuration (maximal misalignment angle $\Delta\theta^{\max} = 30°$) for different values of the bending rigidity constant K_b. Freely-jointed system ($K_b = 0$) is presented as reference. a and ζ are fixed to 1 and ck_BT to 0.1 in a consistent system of units. λ_3 is the rotational diffusion time of a (3-beads)–(rigid-rod) system of equal length

though the loss modulus responses are similar, an interesting difference in the storage modulus is appreciated. In fact, on the one hand the activation of the mild elasticity for the system with a natural bent configuration is observed at a lower characteristic frequency than the system with a straight configuration; on the other hand, a more steeped mild elasticity is noticed for the bent system in comparison with the straight one. In front of this qualitative feature the equilibrium configuration appears a priori as an important factor affecting the dynamic response under flow of a multi bead-rod system.

In Fig. 26 the BD predictions of the complex modulus for a non-freely jointed (three-beads)–(two-rods) system with a natural bent configuration for different values of the bending rigidity constant are presented. The typical thermal-to-flow induced relaxation process occurring around the rotational diffusion time λ_3 (as in the equivalent straight systems) is easily identifiable. Additionally, an interesting second relaxation process (as showed before) activating a mild elasticity at intermediate frequencies is again appreciated for the natural bent systems. BD simulations have showed that the characteristic frequency of this relaxation process and the magnitude of the storage modulus enhancement are function of the bending rigidity constant. The activation frequency of this mild elasticity is increased as the bending rigidity constant is increased as well. This feature is physically coherent taking into account that a higher energy input (i.e. solicitation frequency) is required for activate the first bending mode of a stiffer system. On the other hand, it is also noticed that the storage modulus enhancement and the frequency range associated to those new relaxation processes also rises as the bending rigidity increases. This qualitative feature can be physically explained considering that the stored internal energy associated with a given bending mode is directly proportional to the bending rigidity constant.

5 Summary

Brownian dynamics (BD) is an extensive numerical method for analyzing the dynamic behavior of any coarse-grained structural model. In fact, BD is practically the only mathematical approach for those structural models that do not have an equivalent Fokker-Planck (FP) equation and, in addition, is an alternative approach for solving in a discrete fashion the FP equation of those models that have one. This extensive micro-to-macro approach is purely stochastic and, in consequence, relatively costly in terms of computational resources. A correct implementation of a BD simulation in computational rheology for a given structural model depends particularly on the precise formulation of an equivalent stochastic differential equation coupled with a coherent time integration algorithm and a stress tensor calculation.

This paper tackled the BD simulation of the linear viscoelastic behavior of dilute solution of two classical models in kinetic theory: multi-bead-spring chains and multi-bead-rod chains. An algorithm for simulating a dynamic test in linear viscoelasticity (small-amplitude oscillatory flow) has been developed. The BD approach in linear viscoelasticity for the generalized bead-spring model was validated in front of the analytical solutions of the Rouse theory (freely-jointed multi-bead-(Hookean-springs) chains without hydrodynamic interaction) and Zimm theory (freely-jointed multi-bead-(Hookean-springs) chains with equilibrium-averaged hydrodynamic interaction), implementing a simple Euler time-integration scheme and the Kramers expression for calculating the shear-stress tensor.

On the other hand, the BD simulation in linear viscoelasticity for the generalized bead-rod model was validated with respect to the exact numerical solution for the freely-jointed (three-beads)–(two-rods) chain given by Hassager, implementing an explicit time-integration scheme and the Kramers-Kirkwood expression coupled with a "long-lasting" Brownian forces algorithm for calculating the shear-stress tensor. Moreover, it was shown that a bi-dimensional BD modelling allows to correctly approach the dynamic behavior of classical 3D bead-rod-spring chain models.

The dynamic response of non-freely-jointed multi-bead-rod chains with naturally straight and non-straight configuration was also simulated. In terms of numerical implementation of the naturally non-straight configuration, a mechanically coherent re-definition of the discretized version of the bending potential for naturally straight semi-flexible filaments was necessary in order to tackle properly the cases of bent configurations. An algorithm by decomposing the multi-bead-rod chain in (three-beads)–(two-rods) sub-sections was developed with the aim of calculating the forces coming from the internal bending potential.

From the BD simulation results, non-negligible differences in the rheological responses were found between the naturally straight and the naturally bent models. BD simulation of bead-spring models was demonstrated to be more straightforward than the simulation of bead-rod chains. The presence of physical constraints imposes several restrictions in terms of Brownian forces generation, time-integration algorithms and stress tensor calculation that are reflected directly on the implementation of the BD simulation.

References

1. Kröger M (2005) Models for polymeric and anisotropic liquids. Springer, Berlin
2. Langevin P (1908) Sur la théorie du mouvement Brownien. C R Acad Sci 146:530
3. Öttinger HC (1996) Stochastic processes in polymeric fluids. Springer, Berlin
4. Ermak DL, McCammon JA (1978) Brownian dynamics with hydrodynamic interactions. J Chem Phys 69(4):1352–1360
5. Pear MR, Weiner JH (1980) Brownian dynamics study of a polymer chain of linked rigid bodies. II. Results for longer chains. J Chem Phys 72(7):3939–3947
6. Hatzikiriakos SG, Vlassopoulos D (1996) Brownian dynamics simulations of shear-thickening in dilute polymer solutions. Rheol Acta 35(3):274–287
7. Agarwal US, Bhargava R, Mashelkar RA (1998) Brownian dynamics simulation of a polymer molecule in solution under elongational flow. J Chem Phys 108(4):1610–1617
8. Cass MJ, Heyes DM, English RJ (2007) Brownian dynamics simulations of associating diblock copolymers. Langmuir 23(12):6576–6587
9. Jin S, Collins LR (2007) Dynamics of dissolved polymer chains in isotropic turbulence. New J Phys 9:360
10. Venkataramani V, Sureshkumar R, Khomami B (2008) Coarse-grained modeling of macromolecular solutions using a configuration-based approach. J Rheol 52(5):1143–1177
11. Dwyer JD, Bloomfield VA (1993) Brownian dynamics simulations of probe and self-diffusion in concentrated protein and DNA solutions. Biophys J 65(5):1810–1816
12. Merlitz H, Rippe K, Kienin KV, Langowski J (1998) Looping dynamics of linear DNA molecules and the effect of DNA curvature: a study by Brownian dynamics simulation. Biophys J 74(2I):773–779
13. García de la Torre J, Pérez Sánchez HE, Ortega A, Hernández JG, Fernandes MX, Díaz FG (2003) Calculation of the solution properties of flexible macromolecules: methods and applications. Eur Biophys J 32(5):477–486
14. Kenward M, Dorfman KD (2009) Coarse-grained Brownian dynamics simulations of the 10–23 DNAzyme. Biophys J 97(10):2785–2793
15. Ansell GC, Dickinson E (1986) Brownian dynamics simulation of the fragmentation of a large colloidal floc in simple shear flow. J Colloid Interface Sci 110(1):73–81
16. Xue W, Grest GS (1989) Brownian dynamics simulations for interacting colloids in the presence of a shear flow. Phys Rev A 40(3):1709–1712
17. Heyes DM, Branka AC (1994) Brownian dynamics simulations of self-diffusion and shear viscosity of near-hard-sphere colloids. Phys Rev E 50(3):2377–2380
18. Bijsterbosch BH, Bos MTA, Dickinson E, Van Opheusden JHJ, Walstra P (1995) Brownian dynamics simulation of particle gel formation: from argon to yoghurt. Faraday Discuss 101:51–64
19. Tokuyama M (1999) Effective diffusion model on Brownian dynamics of hard-sphere colloidal suspensions. Physica A 265(3):333–340
20. Miyahara M, Watanabe S, Higashitani K (2006) Modeling adsorption and order formation by colloidal particles on a solid surface: a Brownian dynamics study. Chem Eng Sci 61(7):2142–2149
21. Schmidt M, Patrick Royall C, Van Blaaderen A, Dzubiella J (2008) Non-equilibrium sedimentation of colloids: confocal microscopy and Brownian dynamics simulations. J Phys Condens Matter **20**(49)
22. Mori N, Fujioka H, Semura R, Nakamura K (2003) Brownian dynamics simulations for suspension of ellipsoids in liquid crystalline phase under simple shear flows. Rheol Acta 42(1):102–109
23. Siettos CI, Graham MD, Kevrekidis IG (2003) Coarse Brownian dynamics for nematic liquid crystals: bifurcation, projective integration, and control via stochastic simulation. J Chem Phys 118(22):10149–10156
24. Song YS, Youn JR (2004) Modeling of rheological behavior of nanocomposites by Brownian dynamics simulation. Korea-Australia Rheol J 16(4):201–212
25. Mendes MJ, Schmidt HK, Pasquali M (2008) Brownian dynamics simulations of single-wall carbon nanotube separation by type using dielectrophoresis. J Phys Chem B 112(25):7467–7477
26. Fakhri N, Tsyboulski DA, Cognet L, Weisman RB, Pasquali M (2009) Diameter-dependent bending dynamics of single-walled carbon nanotubes in liquids. Proc Natl Acad Sci USA 106(34):14219–14223
27. Cruz C, Illoul L, Chinesta F, Régnier G (2010) Effects of a bent structure on the linear viscoelastic response of diluted carbon nanotube suspensions. Rheol Acta 49(11):1141–1155
28. Bird RB, Curtiss CF, Amstrong RC, Hassager O (1987) Dynamics of polymer liquids. In: Kinetic theory, 2nd edn, vol 2. Wyley-Interscience, New York
29. Flory PJ (1969) Statistical mechanics of chain molecules. Wiley-Interscience, New York
30. Kirkwood JG (1967) Macromolecules, J.G. Kirkwood collected works. Gordon and Breach, New York
31. Larson RG (1999) The structure and rheology of complex fluids. Oxford University Press, London
32. Nayac R (1998) Molecular simulation of liquid crystal polymer flow: a wavelet-finite element analysis. PhD thesis, MIT, Cambridge, MA, USA
33. Lozinski A, Chauviere C (2003) A fast solver for Fokker-Planck equation applied to viscoelastic flows calculations: 2D FENE model. J Comput Phys 189(2):607–625
34. Lozinski A, Chauviere C, Fang J, Owens RG (2003) Fokker-Planck simulations of fast flows of melts and concentrated polymer solutions in complex geometries. J Rheol 47(2):535–561
35. Chauviere C, Fang J, Lozinski A, Owens RG (2003) On the numerical simulation of flows of polymer solutions using high-order methods based on the Fokker-Planck equation. Int J Mod Phys B 17(1–2):9–14
36. Suen JK, Nayak R, Armstrong RC, Brown RA (2003) A wavelet-Galerkin method for simulating the doi model with orientation-dependent rotational diffusivity. J Non-Newton Fluid Mech 114(2–3):197–228

37. Chauviere C, Lozinski A (2004) Simulation of dilute polymer solutions using a Fokker-Planck equation. Comput Fluids 33(5–6):687–696
38. Ammar A, Ryckelynck D, Chinesta F, Keunings R (2006) On the reduction of kinetic theory models related to finitely extensible dumbbells. J Non-Newton Fluid Mech 134(1–3):136–147
39. Ammar A, Mokdad B, Chinesta F, Keunings R (2006) A new family of solvers for some classes of multidimensional partial differential equations encountered in kinetic theory modeling of complex fluids. J Non-Newton Fluid Mech 139(3):153–176
40. Chinesta F, Ammar A, Falco A, Laso M (2007) On the reduction of stochastic kinetic theory models of complex fluids. Model Simul Mater Sci Eng 15(6):639–652
41. Mokdad B, Pruliere E, Ammar A, Chinesta F (2007) On the simulation of kinetic theory models of complex fluids using the Fokker-Planck approach. Appl Rheol 17(2):26494-1–26494-14
42. Ammar A, Chinesta F, Joyot P (2008) The nanometric and micrometric scales of the structure and mechanics of materials revisited: an introduction to the challenges of fully deterministic numerical descriptions. Int J Multiscale Comput Eng 6(3):191–213
43. Ammar A, Pruliere E, Chinesta F, Laso M (2009) Reduced numerical modeling of flows involving liquid-crystalline polymers. J Non-Newton Fluid Mech 160(2–3):140–156
44. Pruliere E, Ammar A, El Kissi N, Chinesta F (2009) Recirculating flows involving short fiber suspensions: numerical difficulties and efficient advanced micro-macro solvers. Arch Comput Methods Eng 16(1):1–30
45. Leonenko GM, Phillips TN (2009) On the solution of the Fokker-Planck equation using a high-order reduced basis approximation. Comput Methods Appl Math 199(1–4):158–168
46. Ammar A, Normandin M, Daim F, Gonzalez D, Cueto E, Chinesta F (2010) Non-incremental strategies based on separated representations: applications in computational rheology. Commun Math Sci 8(3):671–695
47. Ammar A, Normandin M, Chinesta F (2010) Solving parametric complex fluids models in rheometric flows. J Non-Newton Fluid Mech 165(23–24):1588–1601
48. Mokdad B, Ammar A, Normandin M, Chinesta F, Clermont JR (2010) A fully deterministic micro-macro simulation of complex flows involving reversible network fluid models. Math Comput Simul 80(9):1936–1961
49. Chinesta F, Ammar A, Leygue A, Keunings R (2011) An overview of the proper generalized decomposition with applications in computational rheology. J Non-Newton Fluid Mech 166(11):578–592
50. Laso M, Öttinger HC (1993) Calculation of viscoelastic flow using molecular models: the connffessit approach. J Non-Newton Fluid Mech 47(C):1–20
51. Feigl K, Laso M, Öttinger HC (1995) Connffessit approach for solving a two-dimensional viscoelastic fluid problem. Macromolecules 28(9):3261–3274
52. Hua CC, Schieber JD (1996) Application of kinetic theory models in spatiotemporal flows for polymer solutions, liquid crystals and polymer melts using the connffessit approach. Chem Eng Sci 51(9):1473–1485
53. Laso M, Picasso M, Öttinger HC (1997) 2-D time-dependent viscoelastic flow calculations using connffessit. AIChE J 43(4):877–892
54. Huang ZP, Xu JW, Ren ZF, Wang JH, Siegal MP, Provencio PN (1998) Growth of highly oriented carbon nanotubes by plasma-enhanced hot filament chemical vapor deposition. Appl Phys Lett 73(26):3845–3847
55. Cormenzana J, Ledda A, Laso M, Debbaut B (2001) Calculation of free surface flows using connffessit. J Rheol 45(1):237–258
56. Keunings R (2004) Micro-macro methods for the multiscale simulation of viscoelastic flow using molecular models of kinetic theory. British Society of Rheology, Glasgow, pp 67–98
57. Rouse PE (1953) A theory of the linear viscoelastic properties of dilute solutions of coiling polymers. J Chem Phys 21(7):1272–1280
58. Zimm B (1956) Dynamics of polymer molecules in dilute solution: viscoelasticity, flow birefringence and dielectric loss. J Chem Phys 24(2):269–278
59. Warner HR (1972) Kinetic theory and rheology of dilute suspensions of finitely extensible dumbbells. Ind Eng Chem Fundam 11(3):379–387
60. Treloar LRG (1975) The physics of rubber elasticity. Oxford University Press, London
61. Marko JF, Siggia ED (1995) Stretching DNA. Macromolecules 28(26):8759–8770
62. Higham DJ (2001) An algorithmic introduction to numerical simulation of stochastic differential equations. SIAM Rev 43(3):525–546
63. Somasi M, Khomami B, Woo NJ, Hur JS, Shaqfeh ESG (2002) Brownian dynamics simulations of bead-rod and bead-spring chains: numerical algorithms and coarse-graining issues. J Non-Newton Fluid Mech 108(1–3):227–255
64. Atkinson J, Goh CJ, Phan-Thien N (1983) Bead-spring models for an adsorbed polymer molecule in a shear flow. J Chem Phys 80(12):6305–6317
65. Fetsko SW, Cummings PT (1995) Brownian dynamics simulation of bead-spring chain models for dilute polymer solutions in elongational flow. J Rheol 39(2):285–299
66. Fixman M (1986) Implicit algorithm for Brownian dynamics of polymers. Macromolecules 19(4):1195–1204
67. Kramers HA (1946) The behavior of macromolecules in inhomogeneous flow. J Chem Phys 14(7):415–424
68. Bird RB, Warner HR, Evans DC (1971) Advances in polymer science, vol 8. Springer, Berlin
69. Macosko CW (1994) Rheology. Principles, measurements and applications. VCH, Weinheim
70. Vattulainen I, Ala-Nissila T, Kankaala K (1994) Physical tests for random numbers in simulations. Phys Rev Lett 73(19):2513–2516
71. Kirkwood JG, Riseman J (1948) The intrinsic viscosities and diffusion constants of flexible macromolecules in solution. J Chem Phys 16(6):465–573
72. Thurston GB, Peterlin A (1967) Influence of finite number of chain segments, hydrodynamic interaction, and internal viscosity on intrinsic birefringence and viscosity of polymer solutions in an oscillating laminar flow field. J Chem Phys 46(12):4881–4885
73. Osaki K, Schrag JL, Ferry JD (1972) Infinite-dilution viscoelastic properties of poly(α-methylstyrene). Applications of Zimm theory with exact eigenvalues. Macromolecules 5(2):144–147
74. Fixman M (1986) Construction of Langevin forces in the simulation of hydrodynamic interaction. Macromolecules 19(4):1204–1207
75. Ferry JD (1970) Viscoelastic properties of polymers, 2nd edn. Wiley, New Jersey
76. Liu TW (1989) Flexible polymer chain dynamics and rheological properties in steady flows. J Chem Phys 90(10):5826–5842
77. Hassager O (1974) Kinetic theory and rheology of bead-rod models for macromolecular solutions. J Chem Phys 60(5):2111–2124
78. Fan XJ, Liu TW (1986) Equilibrium and steady-state flow properties of a suspension of freely rotating chains. J Non-Newton Fluid Mech 19(3):303–321
79. Fixman M (1978) Simulation of polymer dynamics. II. Relaxation rates and dynamic viscosity. J Chem Phys 69(4):1538–1545
80. Gottlieb M, Bird RB (1976) A molecular dynamics calculation to confirm the incorrectness of the random-walk distribution for describing the Kramers freely jointed bead-rod chain. J Chem Phys 65(6):2467–2468
81. Pear MR, Weiner JH (1979) Brownian dynamics study of a polymer chain of linked rigid bodies. J Chem Phys 71(1):212–224

82. Fixman M (1978) Simulation of polymer dynamics. I. General theory. J Chem Phys 69(4):1527–1537
83. Helfand E (1979) Flexible vs rigid constraints in statistical mechanics. J Chem Phys 71(12):5000–5007
84. Hinch EJ (1994) Brownian motion with stiff bonds and rigid constraints. J Fluid Mech 271:219–234
85. Grassia PS, Hinch EJ, Nitsche LC (1995) Computer simulations of Brownian motion of complex systems. J Fluid Mech 282:373–403
86. Grassia P, Hinch EJ (1996) Computer simulations of polymer chain relaxation via Brownian motion. J Fluid Mech 308:255–288
87. Pasquali M, Morse DC (2002) An efficient algorithm for metric correction forces in simulations of linear polymers with constrained bond lengths. J Chem Phys 116(5):1834–1838
88. Shankar V, Pasquali M, Morse DC (2002) Theory of linear viscoelasticity of semiflexible rods in dilute solution. J Rheol 46(5):1111–1154
89. Montesi A, Morse DC, Pasquali M (2005) Brownian dynamics algorithm for bead-rod semiflexible chain with anisotropic friction. J Chem Phys 122:084903
90. Morse DC (1998) Viscoelasticity of concentrated isotropic solutions of semiflexible polymers. 1. Model and stress tensor. Macromolecules 31(20):7030–7043
91. Allison SA, McCammon JA (1984) Multistep Brownian dynamics: application to short wormlike chains. Biopolymers 23(2):363–375
92. Ermak DL, McCammon JA (1978) Brownian dynamics with hydrodynamic interactions. J Chem Phys 69(4):1352–1360
93. Doyle PS, Shaqfeh ESG, Gast AP (1997) Dynamic simulation of freely draining flexible polymers in steady linear flows. J Fluid Mech 334:251–291
94. Morse DC (2004) Theory of constrained Brownian motion. Adv Chem Phys 128:65–189
95. Fixman M, Kovac J (1974) Dynamics of stiff chains. II. Freely jointed chain. J Chem Phys 61:4950–4955